earth

MDPI

Article

Disentangling Climate and Demographic Drivers of Urban Heat Risk: A Geographically Weighted Regression Analysis of Zagreb (2001–2024)

Dino Bečić [1,*] and Mateo Gašparović [2]

[1] Department of Geography, Faculty of Science, University of Zagreb, 10000 Zagreb, Croatia
[2] Chair of Photogrammetry and Remote Sensing, Faculty of Geodesy, University of Zagreb, 10000 Zagreb, Croatia; mateo.gasparovic@geof.unizg.hr
* Correspondence: dbecic.geog@pmf.hr

Abstract

Urban heat risk is intensifying globally, yet the relative contributions of climate warming and demographic restructuring to spatiotemporal risk change remain poorly understood, particularly in post-socialist cities experiencing simultaneous thermal intensification and population aging. This study develops a Heat Risk Population Index (HRPI) integrating satellite-derived land surface temperature, CERRA reanalysis air temperature, and census-based demographic sensitivity for 218 Zagreb neighborhood councils (2001–2024). A multi-scale analytical framework combining additive decomposition, enhanced partial correlations, and geographically weighted regression (GWR) was applied to disentangle the drivers of heat risk change. HRPI increased significantly across all neighborhood councils (mean ΔHRPI = 0.197, $p < 0.001$), with strong positive spatial autocorrelation (Moran's I = 0.416). While air temperature change dominated the city-wide mean increase (72.1%), demographic sensitivity change explained the largest share of spatial variance across neighborhood councils (partial r = 0.677 vs. 0.524 for air temperature), driven by spatially heterogeneous demographic transitions—youth out-migration, aging-in-place in southeastern post-socialist estates, and gentrification in central districts. GWR substantially outperformed global OLS (ΔAICc = 60.1; Adj. R^2: 0.649 $\rightarrow$ 0.816), with local demographic effect sizes varying fivefold across the city. These results demonstrate that heat risk drivers operate at distinct spatial scales: climate dominates city-wide magnitude while demographics determine spatial differentiation. Effective adaptation requires universal thermal interventions combined with spatially targeted demographic strategies in identified hotspot neighborhoods. The multi-scale framework is applicable to other post-socialist cities undergoing concurrent climate and demographic change.

Keywords: urban heat risk; geographically weighted regression; demographic sensitivity; post-socialist cities; spatiotemporal vulnerability; Heat Risk Population Index

Check for updates

Academic Editor: Ashraf Dewan

Received: 9 March 2026
Revised: 17 April 2026
Accepted: 21 April 2026
Published: 28 April 2026

Copyright: © 2026 by the authors. Licensee MDPI, Basel, Switzerland. This article is an open access article distributed under the terms and conditions of the Creative Commons Attribution (CC BY) license.

1. Introduction

1.1. Background and Motivation

Climate change, increasing high heat events, and urban population growth concentrating sensitive groups in thermally intensified environments have made urban warming a major environmental health concern [1]. Higher temperatures increase the risk of heat-related disease and death in susceptible groups like children, the elderly, and those

with long-term health issues. Urban heat islands (UHIs) enhance temperature exposure by reducing plant cover, extending impermeable surfaces, and concentrating buildings [2].

Despite increased awareness, Central and Eastern European towns are underrepresented in heat risk research. This divide is crucial because post-socialist cities are changing differently. Demographic aging is faster because fertility rates are low, young people are leaving cities after joining the EU, and urban regeneration is unequal across neighborhoods, affecting thermal exposure and adaptive ability. This happens in Zagreb. From 2001 to 2024, the city's population changed significantly. There is a higher ratio of older persons and a lower percentage of young people. This altered small-scale heat risk patterns. Meanwhile, regional warming worsened. Croatia's summer temperatures were 2.1 °C to 4.7 °C higher than the 1991–2020 average in 2024, Europe's warmest year [3]. Extended atmospheric reanalysis data suggest that Zagreb's July and August average temperatures have risen 3 °C since 2001. This makes understanding city thermal risk distribution even more crucial.

Previous Landsat-derived land surface temperature (LST) and spatial statistics studies in Zagreb showed that urban architecture, built-up intensity, and vegetation structure affect local temperature changes [4]. However, these studies mostly examined the physical thermal environment and ignored how demographic variations affect neighborhood population heat risk over time.

Most heat vulnerability research is cross-sectional, which does not tell us anything about time and assumes demographic–thermal linkages do not alter [5]. New data demonstrates that heat danger varies substantially across a city, requiring spatially detailed frameworks to capture this neighborhood-scale variety. It fills gaps by studying spatiotemporal heat risk dynamics in Zagreb's 218 neighborhood councils from 2001 to 2024.

This study combines thermal exposure parameters (air temperature from regional climate reanalysis and land surface temperature from satellite remote sensing) with demographic sensitivity factors (age structure and population density) to generate a Heat Risk Population Index (HRPI). Due to the lack of neighborhood-level adaptation capacity indicators (income, housing quality, cooling access, social networks) in Croatian census data, the HRPI defines heat vulnerability as exposure-sensitive. Geography Weighted Regression (GWR) models spatially non-stationary demographic and thermal risk change correlations.

This study has four contributions: First, it provides the first longitudinal heat risk variation study in a post-socialist Central European city, filling a major geographic and temporal gap. Second, it models regionally varying demographic restructuring–thermal intensification interactions using GWR, overcoming global spatial stationarity assumptions. Third, it separates city-wide magnitude from spatial explanatory power using decomposition and partial correlation. This shows that driver supremacy is multi-scale. Fourth, it identifies neighborhood council-level priority areas for evidence-based municipal adaptation planning.

1.2. Theoretical Framework

Heat sensitivity research has moved beyond temperature mapping to include physiological, social, and environmental factors. The fundamental study identified vulnerability's primary components: risks, demography, socioeconomic status, the built environment, and health effects. The report also noted health data validation deficiencies [6]. Later research found considerable disparities between physical temperature indicators and social risk patterns in urban hotspot assessments, highlighting the need for more rigorous evaluation frameworks [7]. The elderly, outdoor laborers, and low-income people in inadequate housing had higher heat-related mortality rates [8].

There are severe methodological issues with heat exposure classification. Satellite LST data alone does not adequately reflect how people feel about the weather; it must be

supplemented with weather station air temperature data and behavior data [9]. Thematic assessments in urban planning, ecology, public health, meteorology, and remote sensing reveal a transition from climatology to environmental justice that prioritizes people [10]. Despite criticism of principal component analysis-based heat vulnerability indices' health validation [11], conceptual frameworks emphasize the exposure–sensitivity–adaptive capacity pattern [12]. A recent study emphasizes the importance of emergency department admissions or mortality statistics for a complete vulnerability assessment [13].

Real-world studies reveal that poor populations are more likely to overheat. In Seville, wealthier neighborhoods had 5.6 °C higher daytime temperatures than poor neighborhoods [14]. Australian cities have composite heat exposure indices that link temperature to unemployment and linguistic difficulties [15]. In Portland, minority and low-income residents were more likely to be exposed to heat and had less access to cooling [16]. Similar tendencies were reported in Harare [17]. More than 6 °C temperature variations between socioeconomic groups in Lima demonstrate the Global South cities' unfairness [18]. California's subsidized housing was concentrated in heat-exposed census areas [19].

Methodologies vary by location. The US Heat Vulnerability Index combined health, demographic, and environmental factors [20]. Hospital admission records confirmed the Melbourne index's heat–health prediction [21]. A small-scale neighborhood analysis in Hermosillo used demographic data and satellite LST [22]. Studies in densely populated European cities suggest that dense urban layouts improve energy use but worsen UHI [23]. A regression-based continental study connected European heatwave mortality to nationality and urban expansion [24]. A synthesis of 16 comprehensive reviews found five mapping issues: inadequate heat event categorization, limiting health confirmation, weak spatiotemporal analytical frameworks, no perceived heat indicators, and no three-dimensional urban morphology data [25].

Recent uses have occurred in several cities worldwide. The MOVE vulnerability hypothesis linked urban growth to heat in Abidjan [26]. Philadelphia found exposed and sensitive areas using MODIS LST and census data [27]. The Population Heat Exposure Index for 369 cities indicated that UHI intensity, not demography, increases exposure [28]. Bucharest's multi-criteria Social-Ecological Vulnerability Index had 23 indicators [29]. Principal component analysis was employed to assess Johannesburg ward risk [30]. Equity-focused urban heat mitigation research found that extending tree canopies and boosting albedo are the best approaches to close health gaps [31]. A continental investigation found LST inequality throughout Europe, especially in the south [32]. MODIS time series tracked Shanghai's UHI population heat exposure [33]. Madrid's UHI-vulnerability intersection study informed urban heat–health design frameworks [34]. Heat levels varied greatly in Tehran [35]. Recife's Urban Heat Island Vulnerability Index demonstrated that the center city was in danger due to heat and not enough resources to adapt [36]. Researchers found London's UHI in disadvantaged districts [37]. UHI–vulnerability overlaps were studied in coastal-arid regions [38]. Numerous Mexican cities were mapped for vulnerability [39]. Southeastern US research connected surface UHI to healthcare access [40]. The UHI Combined Thermal Index was invented by Split [41]. Street-scale morphology and sky view were considered in fine-resolution vulnerability assessments [42]. Nebraska rural heat susceptibility differed [43].

Geographically Weighted Regression has improved urban thermal spatial nonstationarity understanding. GWR is superior to global regression models at finding location-dependent associations. Vegetation and water bodies lower temperatures in Austin, San Antonio, Las Vegas, and Ljutomir, Slovenia, whereas impervious surfaces raise them, with impact sizes that vary [44–47]. Methodological advice recommends GWR and multi-scale versions for valid statistics [48]. New research approaches emphasize separating global

model comparison (OLS vs. GWR via AICc) from local coefficient diagnostics (spatial autocorrelation in β, R^2 variability) for comprehensive spatial non-stationarity assessment. Improved partial correlation frameworks that separate predictor contributions and compensate for confounding factors help determine driver importance in spatially heterogeneous urban areas. GWR is used in GIS workflows to map vulnerabilities [49]. In the Guangzhou-Foshan metropolitan area, the Land Cover Zone-Multiscale GWR approach indicated that land cover composition affects temperature more than socioeconomic determinants [50].

Climate change and urbanization increase UHI heat stress and death [51,52]. Regional vulnerability is formed by biophysical factors such as land surface temperature (LST), vegetation, and blue-green infrastructure, as well as socio-demographic factors that affect exposure and adaptive capabilities [53–55]. Spatial non-stationarity requires localized analytical frameworks; GWR with GIS-driven methodologies identifies areas where vegetation cooling does not increase societal vulnerability, emphasizing the need for targeted adoption strategies [56]. Risk assessment and urban design must be combined to make communities resilient [57,58].

1.3. Research Gaps and Study Placement

Despite this wealth of data, gaps remain. First, vulnerability changes over time are rarely studied, especially in post-socialist cities with changing populations and geographies [5,6,10]. Second, most research uses global regression models, which hide neighborhood council-level demographic–temperature connections [7,44,48]. Third, not many frameworks distinguish city-wide magnitude contributions from spatial explanatory power [6,11,25]. They often confuse "what changed most on average" with "what explains spatial differences." Fourth, the absence of adaptive capacity indicators in many contexts, particularly data-limited settings, necessitates reframing vulnerability indices as thermal–demographic exposure metrics requiring cautious interpretation [5,6,12].

This longitudinal GWR-based analysis of Zagreb's heat risk from 2001 to 2024 uses air temperature reanalysis data, satellite LST data, and fine-resolution census data to fill these gaps. Modeling relationships that change over geography and distinguishing the contributions of different scales of drivers produces a methodological framework that may be employed in other circumstances with limited data and helps municipal heat adaptation planning.

1.4. Study Aim and Research Questions

The primary aim of this study is to disentangle the relative contributions of climatic warming and demographic restructuring to changes in urban heat risk across spatial scales in Zagreb between 2001 and 2024. To achieve this aim, the analytical framework examines temporal change, spatial structure, and spatial heterogeneity in heat-related population impacts across urban neighborhood councils.

The study operationalizes heat risk through the Heat Risk Population Index (HRPI), which captures the exposure-sensitivity dimensions of heat vulnerability. Because adaptive capacity indicators are not available at the neighborhood council level in Croatian census data, this limitation is explicitly acknowledged in the index design and interpretation.

Three interconnected research questions guide the analysis:

- RQ1: Has composite heat risk (HRPI) increased across Zagreb (2001–2024), exhibiting spatial clustering rather than random variation (i.e., absence of spatial autocorrelation)?
- RQ2: To what extent do demographic changes (youth and elderly population shifts) versus climatic changes (air and surface temperature increases) predict heat risk change (ΔHRPI), and which component better explains spatial variation across neighborhood councils?

- RQ3: Do heat risk determinant relationships vary geographically within Zagreb, supporting identification of priority intervention areas through spatially non-stationary modeling?

Building on the study objectives and the conceptual distinction between climatic exposure and demographic sensitivity, the following hypotheses are formulated to examine temporal change, spatial structure, and spatial heterogeneity in heat-related population impacts across urban neighborhood councils.

H1. *Temporal Change and Spatial Patterning: ΔHRPI (2001–2024) will be positive on average and exhibit significant positive spatial autocorrelation (Moran's I > 0, p < 0.05). Sub-hypotheses:*

H1a. *Tests whether mean ΔHRPI is significantly greater than zero (paired t-test).*

H1b. *Tests spatial autocorrelation of ΔHRPI (Global Moran's I).*

H2. *Demographic Dominance: Demographic change (ΔDSI) will exhibit stronger spatial explanatory power for ΔHRPI than climatic changes (ΔTair, ΔLST), as evidenced by enhanced partial correlations: $|r(\Delta DSI|\Delta LST, \Delta Tair)| > max(|r(\Delta LST|\Delta DSI)|, |r(\Delta Tair|\Delta DSI)|)$. This hypothesis concerns geographic differences across neighborhood councils, not city-wide average change.*

H3. *Spatial Non-Stationarity and Model Performance: A GWR model will outperform global OLS as evidenced by: (H3a) ΔAICc > 3; (H3b) significant spatial autocorrelation in local β coefficients (Moran's I > 0, p < 0.05); and (H3c) substantial local R^2 variability (SD > 0.10).*

2. Materials and Methods

2.1. Study Area

Zagreb, Croatia's capital with approximately 800,000 residents, displays distinct spatial typologies: a compact historical center with dense pre-war building stock and limited green space; post-socialist medium- and high-rise residential estates concentrated in the inner and mid-ring zones, now housing concentrated elderly populations; and more sparsely populated suburban zones with younger demographic profiles and greater vegetation cover. This morphological heterogeneity generates divergent thermal environments and demographic compositions across short distances.

The north–south topographic gradient, from the forested slopes of Medvednica Mountain (1033 m) to the Sava river floodplain, produces distinct microclimatic regimes. Upslope neighborhood councils benefit from cooler air drainage and canopy cover, while low-lying central and eastern districts accumulate heat through impervious surfaces and anthropogenic heat emissions. Selective demographic aging, suburban growth, and irregular densification have further differentiated local heat risk (Figure 1).

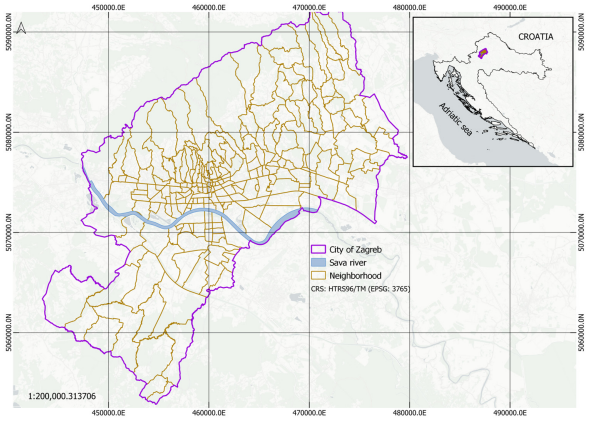


Figure 1. Study area overview.

2.2. Climatic Context

The Copernicus Climate Change Service reported 2024 as the hottest year on record globally, with summer land surface temperatures surpassing the 1991–2020 average by 1.54 °C. Croatia followed this pattern: the Croatian Meteorological and Hydrological Service (DHMZ) classified July and August 2024 as extremely hot, with anomalies of +2.1 °C to +4.7 °C [59,60]. Local measurements confirm intra-urban thermal contrasts: air temperatures averaged 27.2 °C at Zagreb Grič versus 25.1 °C at Maksimir [61]. CERRA reanalysis shows July–August means rising from 21.4–21.6 °C in 2001 to 24.2–24.5 °C in 2024 (+2.8 to +2.9 °C), converging with station data on the conclusion that Zagreb has experienced substantial summer warming [62].

2.3. Data Sources

2.3.1. Air Temperature Data

Air temperature data were obtained from the Copernicus Regional Reanalysis for Europe (CERRA) [63], providing spatially continuous 2 m air temperature (T*air*) at 5.5 km horizontal resolution. T*air* represents the air temperature experienced by outdoor populations and is the epidemiologically relevant thermal metric for heat-related health impacts, driven by synoptic-scale circulation and conceptually distinct from LST. Including both metrics in the HRPI provides complementary thermal information: regional atmospheric forcing (T*air*) and localized surface microclimate (LST), rather than treating either as a standalone proxy [64,65]. The joint use of T*air* and LST also prevents a common interpretive shortcut in UHI studies: treating surface temperature as a direct proxy for ambient thermal exposure. In Zagreb, regional atmospheric warming acts as a largely city-wide baseline, while surface heating varies more strongly with land cover and urban form at sub-kilometer scales. Using both measures allows the HRPI to reflect the shared warming signal experienced across all neighborhood councils and, simultaneously, the micro-spatial thermal contrasts that differentiate neighborhood council risk trajectories.

The July–August seasonal mean T*air* was extracted for 2001 and 2024 from CERRA hourly output as a full 24 h daily average representing peak heat season thermal load. Neighborhood council-level values were derived using bilinear interpolation and area-weighted zonal averaging.

2.3.2. Demographic Data and Projection Validation

Demographic metrics were obtained from the 2001 and 2021 population censuses (Croatian Bureau of Statistics) [66,67], focusing on youth (0–19 years) and elderly (65+) population groups with well-documented elevated heat-related morbidity and mortality risks [68–71]. The DSI focuses on age structure due to the absence of socioeconomic indicators at the mjesni odbor level, a recognized limitation addressed in the Section 4.

To synchronize demographic data with 2024 thermal measurements, age-group shares required projection from 2021 census values. Given documented demographic nonlinearity in post-socialist urban contexts, a retrospective validation framework was implemented to empirically determine the most accurate projection method. The validation uses three census points (2001, 2011, 2021), with 2001–2011 data predicting the known 2021 values across all 218 neighborhood councils as a true out-of-sample test. Five candidate methods (A–E) were considered for the 2024 projection; Methods A and D were excluded from retrospective validation as they cannot be evaluated in the 2001–2011 $\rightarrow$ 2021 holdout framework, leaving Methods B, C, and E as comparable candidates. Three methods were evaluated.

Method B (linear trend): Constant annual change from 2001 to 2011 applied over the subsequent decade.

$$Share_{2021} = Share_{2011} + (Share_{2011} - Share_{2001}) \quad (1)$$

Method C (exponential): Compound annual growth rate applied over ten years.

$$Share_{2021} = Share_{2011} * 1 + (CAGR)^{10}\ CAGR = \left(\frac{Share_{2011}}{Share_{2021}}\right)^{\frac{1}{10}} - 1 \quad (2)$$

Method E (no-projection baseline): 2011 values held constant.

$$Share_{2021} = Share_{2011} \quad (3)$$

Method E achieved best overall performance for both age-group shares (avg R^2 = 0.708, avg RMSE = 3.70 pp), outperforming linear (avg R^2 = 0.594, RMSE = 4.24 pp) and exponential methods (avg R^2 = 0.546, RMSE = 4.47 pp). This result reflects near-zero inter-decadal correlations in demographic change: r = −0.176 for youth share and r = +0.123 for elderly share values near zero indicate that inter-decadal trends lack predictive continuity. Demographic trajectories in Zagreb's post-socialist context are characterized by abrupt reversals driven by migration, gentrification, and new housing development, making trend extrapolation unreliable. Sensitivity analysis (Section 3.4) confirms that core findings remain robust to alternative projection methods. This projection step is implemented to align demographic information with the 2024 thermal observation window and should be understood as a pragmatic, empirically validated solution under intercensal data constraints. The analysis prioritizes temporally consistent comparison and spatial contrasts across neighborhood councils rather than claiming exact point estimates for each neighborhood council's 2024 age shares.

Accordingly, 2024 age-group shares were projected as

$$Share_{2024} = Share_{2021} \quad (4)$$

For total population counts, Method B was applied separately (R^2 = 0.963), as aggregate population trends exhibit substantially greater temporal stability than compositional age structure:

$$Total_{2024} = Total_{2021} + \left[\frac{Total_{2024} - Total_{2021}}{20}\right] * 3 \quad (5)$$

2.3.3. Land Surface Temperature Data

Thermal exposure was measured using Landsat-derived LST from two periods: Landsat-7 ETM+ (2001) and Landsat-9 OLI/TIRS (2024). Cloud-free July–August images were selected to match the CERRA temporal window. Preprocessing included radiometric calibration, atmospheric correction (single-channel algorithm), reprojection to EPSG:3765, and zonal aggregation to neighborhood councils' boundaries. LST captures localized thermal heterogeneity—heat islands, cool parks, and shaded courtyards—at sub-kilometer scales, serving as a validated indicator of surface-level microclimate conditions complementary to T*air*.

2.3.4. Spatial Units

The spatial unit is the neighborhood council (hr. mjesni odbor), Zagreb's most granular level of local self-government. The city's 218 councils provide consistent spatial entities with uniform demographic data across census periods, enabling construction of temporally

consistent metrics without boundary-change distortions. Their fine resolution permits identification of localized patterns that would be obscured at coarser administrative scales.

2.4. Index Construction

The HRPI integrates thermal exposure and demographic sensitivity into a composite metric characterizing the exposure–sensitivity dimension of heat vulnerability [72,73]. Adaptive capacity indicators are unavailable at neighborhood council resolution in Croatian census data; the HRPI, therefore, identifies areas where thermal exposure and demographic sensitivity coincide, rather than constituting a complete vulnerability assessment, consistent with partial vulnerability indices used under comparable data constraints [74–76]. Accordingly, throughout this manuscript, HRPI is interpreted as an exposure–sensitivity heat risk index, not as a complete vulnerability construct, because neighborhood council-level adaptive capacity indicators (e.g., income, housing quality, access to cooling, health status, and social support) cannot be consistently operationalized at this spatial resolution. HRPI, therefore, serves to identify where thermal exposure coincides with demographic sensitivity and how this combined risk changes over time, while explicitly not claiming to quantify health-validated vulnerability.

2.4.1. Index Components

The HRPI comprises four components:

Air temperature (T*air*): Meteorologically grounded ambient thermal forcing is the primary epidemiologically relevant metric.

Land surface temperature (LST): Localized microclimate conditions shaped by urban morphology, complementing T*air* by resolving sub-kilometer thermal heterogeneity.

Demographic Sensitivity Index (DSI): Proportion of physiologically vulnerable residents per neighborhood council.

Population density (Exposure): Total population per km^2, amplifying risk where density is high.

The dual thermal framework (T*air* + LST) avoids conflating surface temperature with ambient air temperature [64,65]: T*air* provides physiologically relevant atmospheric forcing; LST resolves fine-scale surface microclimate variation. Together they represent the thermal component more completely than either alone.

Because the Demographic Sensitivity Index (DSI) is a constituent component of HRPI, its use as a predictor of ΔHRPI introduces a degree of mechanical co-movement by construction. However, the analytical focus of this study is not on causal inference but on spatial differentiation. The partial correlation framework applied in the analysis explicitly addresses this issue by isolating the unique spatial alignment between demographic change and heat risk variation, thereby distinguishing structural association from index-based co-dependence.

2.4.2. Demographic Sensitivity Index (DSI)

For each neighborhood council i and time point t:

$$P_{\text{youth,i,t}} = \frac{Population_{0–19,\ i,\ t}}{Population_{\ total,\ i,\ t}} \quad (6)$$

$$P_{\text{elderly,i,t}} = \frac{Population_{\ 65+,\ i,\ t}}{Population_{\ total,\ i,\ t}} \quad (7)$$

Proportions are globally min-max normalized across both time points, and the DSI is

computed as their arithmetic mean:

$$DSI_{i,t} = \frac{Norm - P_{i,t}^{youth} + Norm - P_{i,t}^{elderly}}{2} \quad (8)$$

2.4.3. Global Temporal Normalization

All four HRPI components are min-max normalized globally across both time points simultaneously:

$$X_{i,t}^{norm} = \frac{X_{i,t} - \min(X_{2001},\ X_{2024})}{\max(X_{2001},\ X_{2024}) - \max(X_{2001},\ X_{2024})} \quad (9)$$

Within-year normalization would, by construction, force each year's distribution to span the full [0, 1] range, artificially ensuring that ΔHRPI reflects only rank changes rather than genuine magnitude differences. Global normalization uses a common reference range from the pooled 2001 and 2024 distributions, allowing ΔHRPI to capture true inter-temporal change.

2.4.4. Index Formula and Temporal Differencing

$$HRPI_{i,t} = \frac{T_{norm,i,t}^{air} + LST_{i,t} + DSI_{i,t} + Exposure_{i,t}}{4} \quad (10)$$

The additive formulation was selected for three reasons. First, it enables transparent linear decomposition of component contributions to ΔHRPI. Second, it avoids the multiplicative collapse whereby a single near-zero component, such as low population density, drives the entire index toward zero regardless of high values in other components, which would misrepresent actual risk conditions. Third, it does not structurally predetermine any component as the dominant driver of change, ensuring that the demographic dominance finding (H2) reflects a genuine empirical signal rather than an index construction artifact.

$$\Delta HRPI_i = HRPI_{i,2024} - HRPI_{i,2001} \quad (11)$$

2.5. Analytical Framework

2.5.1. RQ1: Temporal–Spatial Change Analysis

H1a is tested via paired *t*-test comparing $HRPI_{2001}$ and $HRPI_{2024}$ across all neighborhood councils (n = 218), with H_0: μ_difference = 0 against H_1: μ_difference > 0. H1b is tested via Global Moran's I on ΔHRPI using queen contiguity spatial weights, with significance assessed via a 999-permutation test.

2.5.2. RQ2: Comparative Driver Contribution Analysis

H1a H2 is evaluated through three complementary approaches:

Approach A: Component Decomposition: City-wide mean contributions of each HRPI component to overall change are quantified as percentage shares of total absolute change. This identifies what changed most on average city-wide, which is distinct from what explains spatial variation across neighborhood councils, the substantive question of H2. A component may contribute substantially to city-wide mean change yet exhibit weak spatial explanatory power if its change is spatially uniform; conversely, a component with modest mean contribution may dominate spatial differentiation if its change is highly variable and spatially structured.

Approach B: OLS Model Comparison: Three OLS models are estimated and compared via R^2, Adjusted R^2, and AICc: Full (ΔHRPI~ΔDSI + ΔLST + ΔT_{air}), Demographic-only,

and Climate-only. Standardized beta coefficients from the full model indicate relative importance. Multicollinearity is assessed using VIF < 5.

Approach C: Enhanced Partial Correlations: A residual-based partial correlation method isolates each driver's unique spatial contribution while controlling for confounding [77]: for demographic sensitivity, (1) regress ΔHRPI on ΔLST + Δ*Tair*; retain residuals r_Y; (2) regress ΔDSI on ΔLST + Δ*Tair*; retain residuals r_X; (3) r(ΔDSI | ΔLST, Δ*Tair*) = cor(r_X, r_Y). Analogous steps yield partial correlations for ΔLST and Δ*Tair*, each controlling for ΔDSI. H2 is supported if | r(ΔDSI | ΔLST, Δ*Tair*) | > max(| r(ΔLST | ΔDSI) | , | r(Δ*Tair* | ΔDSI) |). All partial correlations are significance-tested at $p < 0.05$.

An auxiliary regression (ΔDSI~Δ*Tair* + ΔLST) tests potential endogeneity, explaining only 3.8% of ΔDSI variance (Adjusted $R^2 = 0.029$). However, ΔLST carries a significant negative standardized coefficient ($\beta = -0.193$, $p = 0.006$), indicating a modest partial association between surface cooling and demographic change. This most plausibly reflects shared underlying processes; neighborhood councils with stronger LST reductions tend to be greener, lower-density, and subject to different redevelopment trajectories, rather than a direct thermal-to-demographic causal pathway. Residual Moran's I on ΔDSI residuals ($I = 0.142$, $p < 0.001$) confirms that the dominant unexplained ΔDSI variation is spatially structured socio-demographic processes, not thermal forcing. This partial confounding is acknowledged as a caveat in H2 interpretation.

2.5.3. RQ3: Geographically Weighted Regression

H3 is tested via GWR [78–80], estimating location-specific coefficients:

$$\Delta HRPI_i = \beta_0(u_i, v_i) + \beta_{DSI}(u_i, v_i)\Delta DSI + \beta_{LST}(u_i, v_i)\Delta LST + \beta_{Tair}(u_i, v_i)\Delta Tair_i + \epsilon_i \quad (12)$$

This tests whether a single city-wide model adequately characterizes heat risk drivers or whether localized mechanisms require neighborhood council-specific characterization. In this study, GWR is employed as a diagnostic tool for spatial non-stationarity, mapping where predictor–outcome associations strengthen or weaken across the city. Local coefficients are therefore interpreted as geographically differentiated relationships rather than as causal effect estimates. The rationale for expecting spatial non-stationarity is grounded in Zagreb's morphological heterogeneity: historic center neighborhood councils, post-socialist estates, and suburban zones likely exhibit distinct demographic–thermal risk relationships.

Five GWR specifications were estimated and compared via AICc. Model 2b (ΔHRPI~ΔYouth + ΔElderly + ΔLST + ΔT_{air} + ΔExposure) is excluded from substantive interpretation despite its nominally superior fit (AICc = −13,179, Adj. $R^2 = 1.000$): ΔExposure is a direct HRPI constituent, making its inclusion circular; substantial multicollinearity ($r = -0.68$ between ΔYouth and ΔElderly; ΔExposure redundant with demographic terms) produces a near-singular design matrix yielding spurious perfect fit rather than genuine explanatory power. The primary specification (Model 1c: ΔHRPI~ΔDSI + ΔLST + ΔT_{air}) was selected based on the lowest AICc among numerically stable models, theoretical coherence, and interpretability. Optimal bandwidth is determined by leave-one-out cross-validation minimizing:

$$\mathrm{CV(b)} = \sum_i [y_i - \hat{y}_{\neq i}(b)]^2 \quad (13)$$

using a bisquare adaptive kernel. AICc-based selection is used as a fallback if cross-validation fails to converge.

The Breusch–Pagan test was applied to OLS residuals prior to GWR estimation. Even in the absence of formal heteroskedasticity, the primary motivation for GWR remains that spatial non-stationarity predictor–outcome relationships may vary geographically

even when global error variance is homoskedastic, as the two conditions address distinct modeling assumptions [80].

H3a. *$\Delta AICc = AICc_OLS - AICc_GWR > 3$ provides substantial evidence favoring GWR [79], penalizing GWR's higher effective degrees of freedom to ensure improvement reflects genuine explanatory gain.*

H3b. *Global Moran's I on local β_DSI coefficients tests for systematic geographic patterning ($I > 0$, $p < 0.05$), confirming structured spatial variation rather than random noise.*

H3c. *SD(Local R^2) > 0.10 indicates geographic heterogeneity in model explanatory power. High local R^2 in peripheral neighborhood councils reflects demographic and thermal changes operating straightforwardly in simplified contexts; lower local R^2 in central mixed-use zones reflects genuine complexity from unmeasured factors. Local R^2 measures predictive performance for ΔHRPI, not the validity of the HRPI as a representation of actual heat-related health outcomes; the absence of external validation against mortality or hospital admissions data is an explicit limitation discussed in Section 5.*

Additional diagnostics included: OLS vs. GWR coefficient comparison quantifying non-stationarity magnitude; residual Moran's I; and a dominant driver typology classifying each neighborhood council as "Demography-driven" ($|\beta_DSI \times \Delta DSI| > |\beta_LST \times \Delta LST + \beta_T_{air} \times \Delta T_{air}$ or "Climate-driven" otherwise.

All analyses were performed using QGIS (v3.26) and RStudio (v2023.09.1 Build 494).

3. Results

This section presents findings organized around three research questions. RQ1 examines temporal and spatial patterns of heat risk change in Zagreb (2001–2024). RQ2 assesses the comparative contributions of demographic and climatic drivers at the city-wide scale. RQ3 analyzes local-scale spatial heterogeneity through geographically weighted regression. All six hypotheses (H1a, H1b, H2, H3a, H3b, H3c) were supported. The presentation proceeds from city-wide aggregate patterns through driver decomposition to spatially explicit local modeling, building a multi-scale understanding of how and why heat risk changed differentially across Zagreb's 218 neighborhood councils over the study period.

3.1. Spatial and Temporal Patterns of Heat Risk Change (RQ1)

The HRPI increased from a mean of 0.338 in 2001 to 0.535 in 2024 on a city-wide scale, resulting in an absolute change (ΔHRPI) of 0.197 units. This increase was statistically significant ($t_{216} = 100.94$, $p < 0.001$, 95% CI = [0.193, 0.201]), as corroborated by a paired *t*-test. All 218 neighborhood councils demonstrated positive change. The systematic nature of the increase is reflected in the narrow confidence interval and large t-statistic. Throughout the study period, no neighborhood council experienced a decrease in composite heat risk, suggesting that the combined effect of demographic aging and warming temperatures was a city-wide structural shift rather than a localized phenomenon. This offers robust empirical support for Hypothesis H1a. Table 1 provides descriptive statistics for ΔHRPI.

Table 1. Descriptive statistics of ΔHRPI (2001–2024).

n	Mean_2001	Mean_2024	Mean_Delta	Sd_Delta	Min_Delta	Median_Delta	Max_Delta	Cv_Delta
218	0.3382	0.5351	0.1969	0.0287	0.1054	0.2004	0.2756	0.1459

Spatial heterogeneity was substantial, despite this universal increase. The coefficient of variation for ΔHRPI was 0.146, and it ranged from 0.105 to 0.276. While the majority

of neighborhood councils experienced moderate increases, a subset of anomalies drove spatial differentiation, as evidenced by the interquartile range (0.036) being narrow relative to the mean (0.197).

Hypothesis H1b was supported by the significant positive spatial autocorrelation in ΔHRPI (I = 0.416, Z = 10.24, $p < 0.001$), which markedly exceeded the expected value under spatial randomness (E[I] = −0.005), as revealed by Global Moran's I. The observed Moran's I exceeded its null expectation by a factor of approximately 83, indicating a significant degree of clustering. This robust positive autocorrelation suggests that neighborhood councils with substantial increases in heat risk are clustered together rather than being dispersed arbitrarily throughout the city. Clustering patterns indicate that spatially structured processes, including demographic contagion (synchronized aging or youth exodus in neighboring areas), land-use spillovers (thermal changes in one neighborhood council affecting adjacent zones), and shared infrastructure deficits, operate across neighborhood council boundaries and produce spatially coherent risk trajectories. This spatial dependence also violates the independence assumption of ordinary least squares regression, which provides methodological justification for the geographically weighted regression approach.

The spatial distribution of HRPI in 2001, 2024, and ΔHRPI is depicted in Figure **??**, which reveals three distinct clusters of elevated change: southeastern post-socialist housing estates (Dugave, Travno, Sloboština; ΔHRPI > 0.24), which are driven by synchronized aging-in-place among residents who settled these mass housing complexes during the 1970s–1980s; southern peri-urban zones (Vrbani, Ivanja Reka, Kobiljak; ΔHRPI > 0.25), which are a reflection of the inadequate cooling infrastructure that accompanied recent suburban expansion; and western industrial corridors (ΔHRPI = 0.18–0.22), which are associated with persistent thermal exposure from impervious surfaces. The tiniest increases (ΔHRPI < 0.13) were observed in central neighborhood councils that were undergoing gentrification. This was due to the fact that younger, higher-income in-migrants had a greater adaptive capacity.

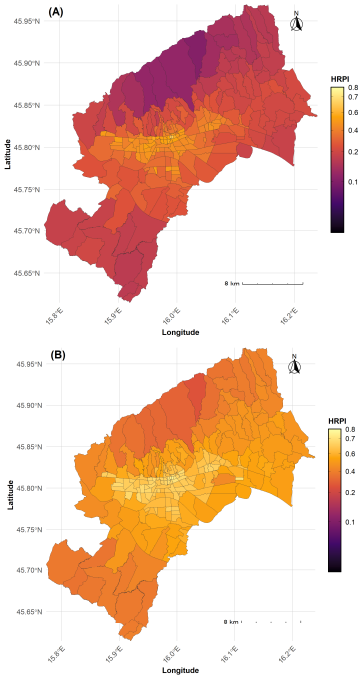


Figure 2. *Cont.*

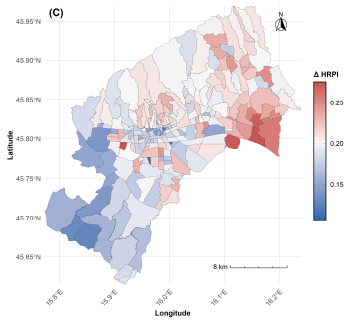


Figure 2. Temporal panels: HRPI in 2001 (**A**), HRPI in 2024 (**B**), and ΔHRPI 2001–2024 (**C**). HRPI increased universally across all neighborhood councils between 2001 and 2024, with the most pronounced increases concentrated in southeastern housing estates and peri-urban zones.

3.2. Drivers of Heat Risk Change: City-Wide Analysis (RQ2)

3.2.1. Component Decomposition

The additive HRPI framework enables the direct decomposition of ΔHRPI into contributions from four components. The magnitude and spatial structure of the city-wide mean contributions are starkly different. Air temperature change was the primary factor in the city-wide average (ΔT_{air} = 0.568, 72.1% of total ΔHRPI), which is consistent with the regional warming trend that was documented in CERRA reanalysis data (+2.8 to +2.9 °C in July–August means between 2001 and 2024) as a common baseline forcing that relatively impacted all neighborhood councils. Urban development intensified impervious surface coverage and reduced vegetation in expanding peripheral zones, resulting in a 29.0% contribution from land surface temperature (ΔLST = 0.228). Demographic sensitivity contributed ΔDSI = 0.018 (2.3%), a modest city-wide average that conceals substantial spatial variance. However, some neighborhood councils experienced increases exceeding 0.20, while others remained near zero. The negative contribution of spatial exposure (ΔExposure = −0.027, −3.4%) was due to the localized increase in green space in specific districts, which partially negated the expansion of heat-retaining surfaces elsewhere.

This decomposition demonstrates that the greatest proportion of the increase in the city-wide mean heat risk is attributable to changes in air temperature. Nevertheless, the spatial covariation; the extent to which component changes are correlated with ΔHRPI across neighborhood councilsand is not captured by the city-wide mean contributions. A component that significantly contributes to the city-wide mean may demonstrate limited spatial explanatory power if its change is spatially uniform. Conversely, a component with a modest mean contribution may dominate spatial differentiation if its change is highly variable and consistent with heat risk patterns. This distinction is essential for the interpretation of Hypothesis H2.

Although air temperature dominates the city-wide mean increase in HRPI, this does not imply that air temperature is the principal driver of spatial differentiation in ΔHRPI. Decomposition answers the question “what changed most on average across the city,” whereas variance-oriented analyses address “what explains why some neighborhood councils increased more than others.” A factor may contribute strongly to the mean shift yet explain little inter-neighborhood council variation if its change is spatially uniform. Conversely, a factor with modest mean contribution can dominate spatial differentiation if it is highly variable and spatially structured. This interpretive separation is critical for avoiding conflation of magnitude-based dominance with variance-based explanatory power.

3.2.2. OLS Regression and Multicollinearity

The explanatory power of demographic versus climatic predictors for spatial variance in ΔHRPI across neighborhood councils was evaluated using three OLS models

(Table 2). The complete model (ΔHRPI~ΔDSI + ΔLST + Δ*Tair*) attained R^2 = 0.654 (adjusted R^2 = 0.649, AIC = −1145.72), suggesting that these three predictors collectively account for 65.4% of the spatial variance in heat risk change. The climate-only model (ΔHRPI~ΔLST + Δ*Tair*) explained R^2 = 0.361 (adjusted R^2 = 0.355, AIC = −1014.84), while the demographic-only model (ΔHRPI~ΔDSI) explained R^2 = 0.184 (adjusted R^2 = 0.180, AIC = −963.84). The full model was identified as preferable by the AIC model selection, confirming that both predictor groups contribute unique explanatory power and should be retained jointly. The complete model's R^2 (65.4%) is significantly greater than the aggregate of the individual R^2 values (18.4% + 36.1% = 54.5%), suggesting that the predictors make synergistic explanatory contributions when they are modeled in conjunction. The relative relevance of predictors under mutual control is quantified by the standardized beta coefficients from the full model. The standardized coefficient for air temperature change was the highest (β = 0.608, $p < 0.001$), followed by demographic sensitivity (β = 0.552, $p < 0.001$) and land surface temperature (β = 0.520, $p < 0.001$). The decomposition's emphasis on air temperature dominance is in stark contrast to the similar magnitudes of standardized coefficients (0.520–0.608), which suggest their comparably significant roles when controlling for other predictors. This distinction is due to the fact that decomposition measures mean contribution, whereas standardized coefficients measure unique spatial covariation.

Table 2. OLS model comparison (Full, Demographic only, Climate only).

Model	R^2.	Adj_R2	AIC
Full (Demographic + Climate)	0.6536	0.6487	−1145.72
Demographic only (ΔDSI)	0.1842	0.1804	−963.84
Climate only (ΔLST + Δ*Tair*)	0.3609	0.3550	−1014.84

Variance inflation factors (VIF) verified that there was negligible multicollinearity among all three predictors: ΔDSI (VIF = 1.04), ΔLST (VIF = 1.10), and ΔTair (VIF = 1.08), all of which are significantly lower than the conventional threshold of 5.0 (Table 3). These low VIF values confirm that predictors are adequately independent of one another, thereby validating that standardized coefficients and partial correlations in subsequent analyses reflect genuine unique contributions rather than confounded shared variance.

Table 3. Variance inflation factors (multicollinearity diagnostic).

Predictor	VIF
delta_DSI	1.040
delta_LST	1.103
delta_T*air*	1.076

3.2.3. Partial Correlations

Partial correlation analysis, which directly tests Hypothesis H2 (demographic dominance in explaining spatial variance), isolates the unique spatial explanatory contribution of each predictor by statistically controlling for the others. The strongest partial correlation (r = 0.677, $p < 0.001$, n = 218) was observed for demographic sensitivity change (ΔDSI), which accounted for 45.8% of unique spatial variance after controlling for both climate predictors (ΔLST and Δ*Tair*). Climatic predictors, which were adjusted for demographic sensitivity, demonstrated reduced partial correlations: Δ*Tair* (r = 0.524, $p < 0.001$, unique variance 27.4%) and ΔLST (r = 0.393, $p < 0.001$, unique variance 15.5%). Hypothesis H2 is supported by the demographic partial correlation, which outperformed the strongest climatic partial correlation by a ratio of 1.29:1. This discovery establishes a critical interpretive distinction. In this context, demographic dominance refers to explanatory power over

spatial variability across neighborhood councils rather than contribution to aggregate city-wide heat risk magnitude. Although the majority of the city-wide mean heat risk increase (72.1% in the decomposition) is attributed to climatic factors, particularly air temperature, demographic factors account for the greatest share of spatial variance, which explains why certain neighborhood councils experienced substantially larger increases than others. The air temperature serves as a uniform baseline forcing that increases the risk of heat in the entire city, but it does not significantly differentiate neighborhood councils. In contrast, demographic sensitivity is highly variable across space, with gentrifying central districts and high-aging estates representing opposing extremities of demographic change. This demographic dominance in partial correlations is driven by the spatial variance in demographic change, which is consistent with heat risk patterns. The direct policy implication is that universal climate adaptation measures are necessary to address the common thermal forcing, while spatially targeted demographic interventions are necessary to reduce spatial inequalities in heat risk outcomes.

3.2.4. Spatial Distribution

The spatial distribution of Δ*Tair*, ΔLST, and ΔDSI is depicted in Figure 3, which serves as visual confirmation of the patterns that were identified through partial correlations and decomposition. The spatial variation of the air temperature change (Figure 3A) was minimal, with nearly all neighborhood councils experiencing increases of 0.36–0.75 °C. This nearly uniform distribution confirms that air temperature is a common forcing factor with a limited ability to differentiate neighborhood council trajectories. Moderate spatial structure was observed in the land surface temperature change (Figure 3B). Southern industrial zones and peri-urban expansion areas experienced elevated increases (ΔLST > 0.35 °C and ΔLST > 0.30 °C, respectively), while northern forested zones and central districts with increased vegetation coverage experienced smaller increases (ΔLST < 0.20 °C).

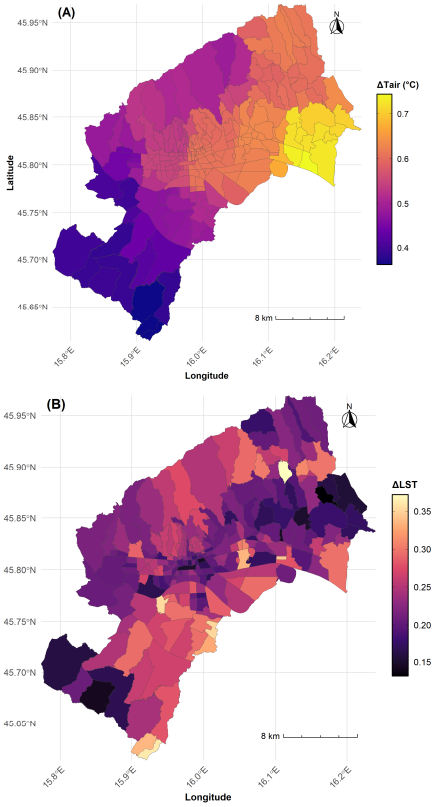


Figure 3. *Cont.*

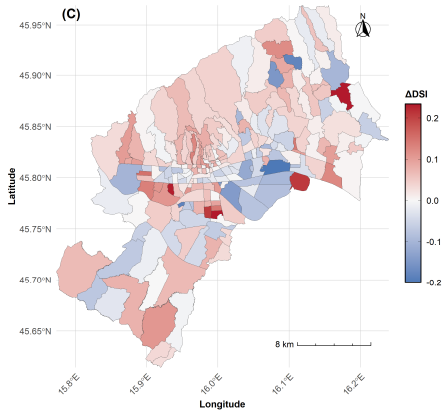


Figure 3. Spatial distribution of Δ*Tair* (**A**), ΔLST (**B**), and ΔDSI (**C**). While air temperature change is spatially uniform, land surface temperature and demographic sensitivity exhibit strong spatial variability, supporting their role in explaining differences in heat risk across neighborhood councils.

The demographic sensitivity change (Figure 3C) demonstrated the most severe spatial differentiation, with significant increases in southeastern housing estates (ΔDSI > 0.20) and western peripheral zones, and modest increases or decreases in central districts that are undergoing gentrification (ΔDSI < 0.05). The dominance of demographic sensitivity in partial correlations is ascribed to the high spatial variance, despite the modest city-wide mean (0.018). The spatial clustering of demographic change (Moran's I = 0.137, Z = 3.44, $p < 0.001$) corroborates the spatial structure of demographic transitions. Southeastern estates form a contiguous cluster of high ΔDSI, which is driven by synchronized aging among residents who originally settled these complexes in the 1970s–1980s. Central neighborhood councils form a contiguous cluster of low ΔDSI, which is driven by coordinated gentrification and urban renewal.

3.3. Geographically Weighted Regression (RQ3)

3.3.1. Model Selection and GWR Superiority

Five GWR model specifications were estimated and contrasted using AICc (see Table 4). Model 1c (ΔHRPI~ΔDSI + ΔLST + Δ*Tair*) attained the lowest AICc among numerically stable models (AICc = −1205.7, adjusted R^2 = 0.816, bandwidth = 27 neighbors), which represents a marked improvement over Model 1a (ΔAICc = 124.1) and Model 1b (ΔAICc = 18.1). A bandwidth of 141 neighbors (65% of the dataset) was required by Model 2a, which effectively approximated global model behavior and undermined the local specificity that substantiates GWR. Due to the circular inclusion of Δexposure, a direct HRPI constituent as a predictor, in conjunction with the multicollinearity-induced near-singular design matrix, Model 2b exhibited a spurious perfect fit (Adj. R^2 = 1.000, AICc = −13,179.9). Consequently, it is excluded from interpretation. The primary specification was chosen based on the empirical performance, bandwidth stability (27 neighbors enabling genuinely local estimation), and theoretical parsimony of the composite DSI, which captures the aging-in-place demographic transition more coherently than disaggregated youth and elderly predictors. Model 1c was adopted.

Table 4. GWR model selection.

Model	Predictors	BW	AICc	Adj_R2
1a	DSI	23	−1081.55	0.618
1b	DSI + LST	30	−1187.63	0.776
1c	DSI + LST + T*air*	27	−1205.67	0.816
2a	Youth + Elderly + LST + T*air*	141	−1188.70	0.724
2b	Youth + Elderly + LST + T*air* + Exposure	141	−13,179.89	1.000

The null hypothesis of homoskedasticity was not rejected by the Breusch–Pagan test, which was conducted on OLS residuals prior to GWR estimation, resulting in BP = 5.39 (df = 3, p = 0.145). As previously mentioned, the absence of formal heteroskedasticity does not preclude GWR. The primary motivation remains spatial non-stationarity in predictor–outcome relationships, which is fully compatible with homoskedastic global residuals, as the two conditions address fundamentally distinct modeling assumptions.

A significant advance is evident in the comparison of GWR Model 1c to the global OLS baseline. AICc = −1145.5 was attained by the global OLS model, while ΔAICc = 60.1 was obtained by GWR Model 1c at AICc = −1205.7. A difference exceeding 10 is considered decisive evidence in favor of the model with a lower AICc, according to standard AICc interpretation guidelines. A difference of 60.1 suggests that the global model receives virtually no empirical support in comparison to GWR. The adjusted R^2 improvement (OLS: 0.649 → GWR: 0.816) signifies a 48% reduction in residual variance, which corroborates the robust support for Hypothesis H3a and establishes that predictor–outcome relationships differ significantly across communities.

3.3.2. Spatially Varying Coefficients

The global OLS coefficients and GWR local coefficient distributions for Model 1c are compared in Table 5. The global OLS model estimated a single citywide coefficient (β_DSI = 0.223, SE = 0.017, $p < 0.001$) for demographic sensitivity, suggesting a uniform effect across all communities. The demographic sensitivity effect on heat risk varies by a factor of approximately five across the city, as evidenced by the considerable heterogeneity in this relationship that GWR revealed: local β_DSI ranged from −0.079 to +0.393 (mean = 0.223, SD = 0.074, CV = 0.332). In 90% of neighborhood councils (n = 196), β_DSI was statistically significant and positive. In 10% (n = 21), it was near-zero or weakly negative, likely indicative of contextual factors in which aging populations were protected from heat risk consequences by superior adaptive capacity, social support networks, or public health infrastructure. The land surface temperature coefficients demonstrated even greater heterogeneity, with a range of −0.191 to +0.925 (mean = 0.342, SD = 0.191, CV = 0.560). The air temperature coefficients exhibited extreme variation (range = −7.11 to +6.17, CV = 14.89), which is indicative of estimation instability due to the predictor's near-uniform spatial distribution. In the event that a predictor has low spatial variance, GWR is unable to reliably estimate meaningful local effects.

Table 5. Comparison of global (OLS) vs. local (GWR) coefficients: range, mean, standard deviation, and coefficient of variation.

Predictor	OLS_Beta	GWR_Mean	GWR_SD	GWR_Range
delta_DSI	0.2233	0.2233	0.0741	0.472
delta_LST	0.3459	0.3419	0.1913	1.116
delta_T*air*	0.2327	0.0602	0.8971	13.274

The observed variability in local coefficient estimates is an expected property of GWR models, reflecting underlying spatial non-stationarity in predictor–outcome relationships. In spatially heterogeneous urban systems, coefficients are not assumed to be constant but are allowed to vary across locations, often resulting in substantial differences in magnitude and, in some cases, direction [78,79].

Previous studies applying GWR to urban temperature and environmental variables have similarly reported strong spatial variability in coefficient estimates, particularly for land cover and socio-demographic predictors, confirming that such patterns reflect genuine geographic differentiation rather than model instability [44–47].

Local β_DSI, β_LST, and β_T*air* coefficients are depicted in Figure 4. The β_DSI values of the southeastern housing estates (Dugave, Travno, Sloboština) were the highest (>0.35), suggesting that demographic aging resulted in disproportionately large heat risk increases in areas characterized by poor housing quality, limited air conditioning penetration, aging building stock, and inadequate elderly support services. Central gentrifying neighborhood councils (Donji grad, Trnje) exhibited the lowest β_DSI (<0.15), which is indicative of the attenuation of the impact of demographic aging by higher socioeconomic status and improved adaptive infrastructure.

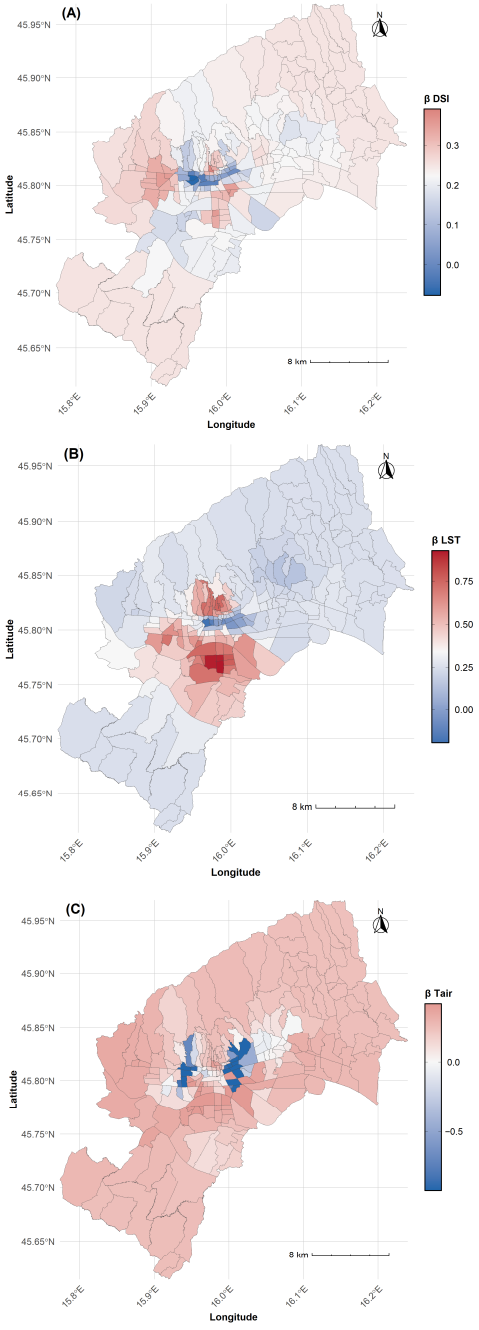


Figure 4. Spatial distribution of local GWR coefficients: β_DSI (**A**), β_LST (**B**), and β_T*air* (**C**). The spatial distribution of local GWR coefficients reveals substantial heterogeneity, with the strongest demographic effects concentrated in southeastern estates and weaker effects in central districts.

In support of Hypothesis H3b, the application of Global Moran's I to local β_DSI coefficients revealed a strong positive spatial autocorrelation (I = 0.647, Z = 15.95, $p < 0.001$).

This finding confirms that neighborhood councils with similar demographic sensitivity effects cluster geographically rather than distribute arbitrarily. This spatial structure suggests that the underlying contextual factors; housing typology, socioeconomic composition, and public service availability—spatially aggregate and systematically alter the way in which demographic aging is translated into heat risk. The standardized construction with poor thermal insulation, limited green space, and concentrated populations of original residents now in their 60s–70s are all shared characteristics of socialist-era mass housing, as evidenced by the contiguous cluster of high β_DSI in southeastern estates. Coordinated policy interventions that target these zones can therefore accomplish disproportionate heat risk reductions by simultaneously addressing common structural deficits across multiple neighboring high-sensitivity areas.

3.3.3. Local Model Fit

Local R^2 quantifies the proportion of variance in ΔHRPI that is explained by the three predictors within each neighborhood council's local regression window, thereby providing a spatially explicit measure of model performance. The mean local R^2 was 0.881, with a standard deviation of 0.112, and it varied from 0.441 to 1.000 across 218 communities. The model's explanatory power was confirmed by the standard deviation exceeding the 0.10 threshold established for Hypothesis H3c, which supports H3c and demonstrates significant geographic heterogeneity. In nearly half of the neighborhood councils ($R^2 > 0.95$, n = 108, 49.8%), the demographic–climatic predictor set very effectively explained the change in heat risk. A lower fit in 21.2% of neighborhood councils ($R^2 < 0.80$, n = 46) suggests that unmeasured factors, such as daytime population exposure, building-level adaptive capacity, socioeconomic status, or healthcare accessibility, are contributing factors. These central industrial and mixed-use neighborhood councils are contexts in which the three-predictor model necessitates the inclusion of additional variables in future research.

R^2 values near 1.000 in peri-urban and peripheral districts indicate simplified land-use contexts in which demographic and thermal changes operate without confounding from unmeasured socioeconomic or infrastructural complexity, rather than model overfitting. The bimodal distribution between high-fit peripheral areas and lower-fit central zones is illustrated by the embedded histogram in Figure 5, which depicts local R^2 values.

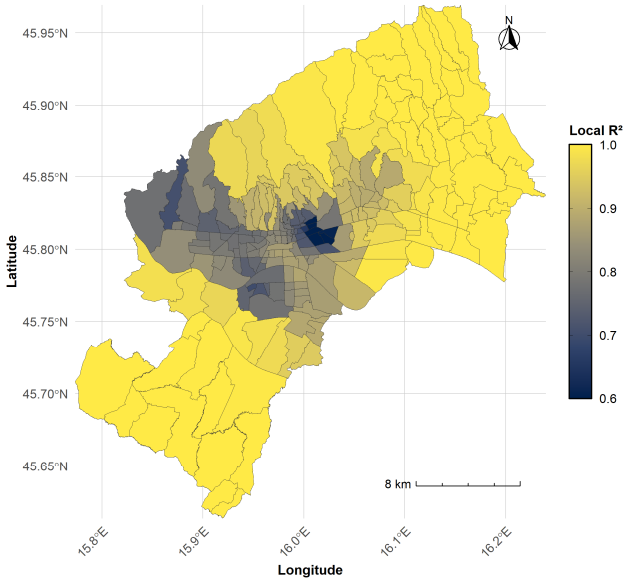


Figure 5. Map of local R^2 values (GWR Model 1c). Local model performance varies across the city, with higher explanatory power in peripheral areas and lower values in complex central urban zones.

3.3.4. Residual Spatial Autocorrelation

Residual spatial autocorrelation is a critical diagnostic for spatial regression models. The presence of significant clustering in the model residuals suggests that the model has failed to represent spatially structured processes, which could potentially bias the inference. Global Moran's I was applied to the residuals of GWR Model 1c, and the results were negligible autocorrelation (I = 0.050, Z = 1.35, p = 0.089), which did not surpass the significance threshold (Table 6). The spatial structure of heat risk change was effectively captured by GWR, as evidenced by the near-zero Moran's I, which is only marginally above the null expectation of E[I] = −0.005. This leaves only non-spatial idiosyncratic variation unexplained. This confirms that the hypothesis tests and coefficient interpretations discussed above are not influenced by unaccounted spatial dependence (Table 6). The low magnitude of Moran's I is expected in this context and indicates that spatial dependence has been effectively accounted for by the GWR model. In spatial regression diagnostics, near-zero residual autocorrelation is interpreted as evidence of a well-specified model where spatially structured variation has been successfully captured, leaving only random, non-spatial residual variation.

Table 6. Residual spatial autocorrelation (Moran's I, GWR Model 1c).

Model	Moran_I	Expected	Z-Score	*p*_Value
GWR Model 1c	0.0503	−0.0046	1.35	0.0886

3.3.5. Dominant Driver Classification

The classification of each neighborhood council was determined by the largest absolute local contribution to ΔHRPI: $|\beta_DSI \times \Delta DSI|$, $|\beta_LST \times \Delta LST|$, or $|\beta_T air \times \Delta T air|$. The findings indicated that climate-driven neighborhood councils (n = 196) comprised 90.3% of the sample, while demography-driven neighborhood councils (n = 21) comprised 9.7%. This result does not contradict the previous result of demographic dominance in partial correlations (Section 3.2.3), as the two analyses address fundamentally distinct questions. The predictor that best explains spatial variance across localities is demographics (r = 0.677), as demographic change varied significantly across space, aligning with heat risk patterns. Partial correlations are used to determine this. The dominant driver classification identifies the predictor that has the greatest absolute local effect within each neighborhood council. The answer is climate (90%), as air temperature has contributed significant absolute increases uniformly across the city, despite the fact that this uniform contribution explains little spatial differentiation. The prevalent driver typology is depicted in Figure 6.

The multi-scale synthesis that results is as follows: Air temperature serves as a common baseline forcing, contributing the most significant mean increase (72.1% of decomposition) at the city-wide level. Demographics account for the most significant differentiation (partial r = 0.677) at the spatial variance scale, thereby identifying the neighborhood councils that experience disproportionate increases. At the local absolute contribution scale, demographics dominate the 9.7% of critical high-heat risk zones that require targeted intervention, while climate dominates 90.3% of communities. Universal climate measures; urban greening, cool surfaces, and shade structures that address the common thermal forcing, in conjunction with spatially targeted demographic interventions such as elderly support services, youth retention programs, and neighborhood council-level health infrastructure—to address differentiation hotspots, are necessary for effective adaptation.

To enhance the policy operability of the findings, a thermal risk intervention priority matrix was constructed using ΔHRPI and local β_DSI values (Figure 7). Median thresholds were used to distinguish between high and low values, resulting in four distinct neigh-

borhood council types. The high risk–high sensitivity quadrant (Priority 1) represents critical intervention zones where both heat risk increase and demographic vulnerability are elevated. These areas require integrated interventions combining thermal mitigation and targeted demographic support. The high risk–low sensitivity quadrant (Priority 2) captures climate-driven risk areas where heat exposure increases are substantial but demographic sensitivity remains moderate, suggesting prioritization of physical mitigation strategies such as urban greening and cooling infrastructure. The low risk–high sensitivity quadrant (Priority 3) represents latent vulnerability zones, where current heat risk increase is moderate but demographic sensitivity is high, indicating potential future risk escalation. Finally, the low risk–low sensitivity quadrant (Priority 4) includes relatively stable areas with limited immediate intervention needs. This classification translates the multi-scale analytical framework into actionable spatial categories, supporting more targeted and efficient allocation of adaptation measures.

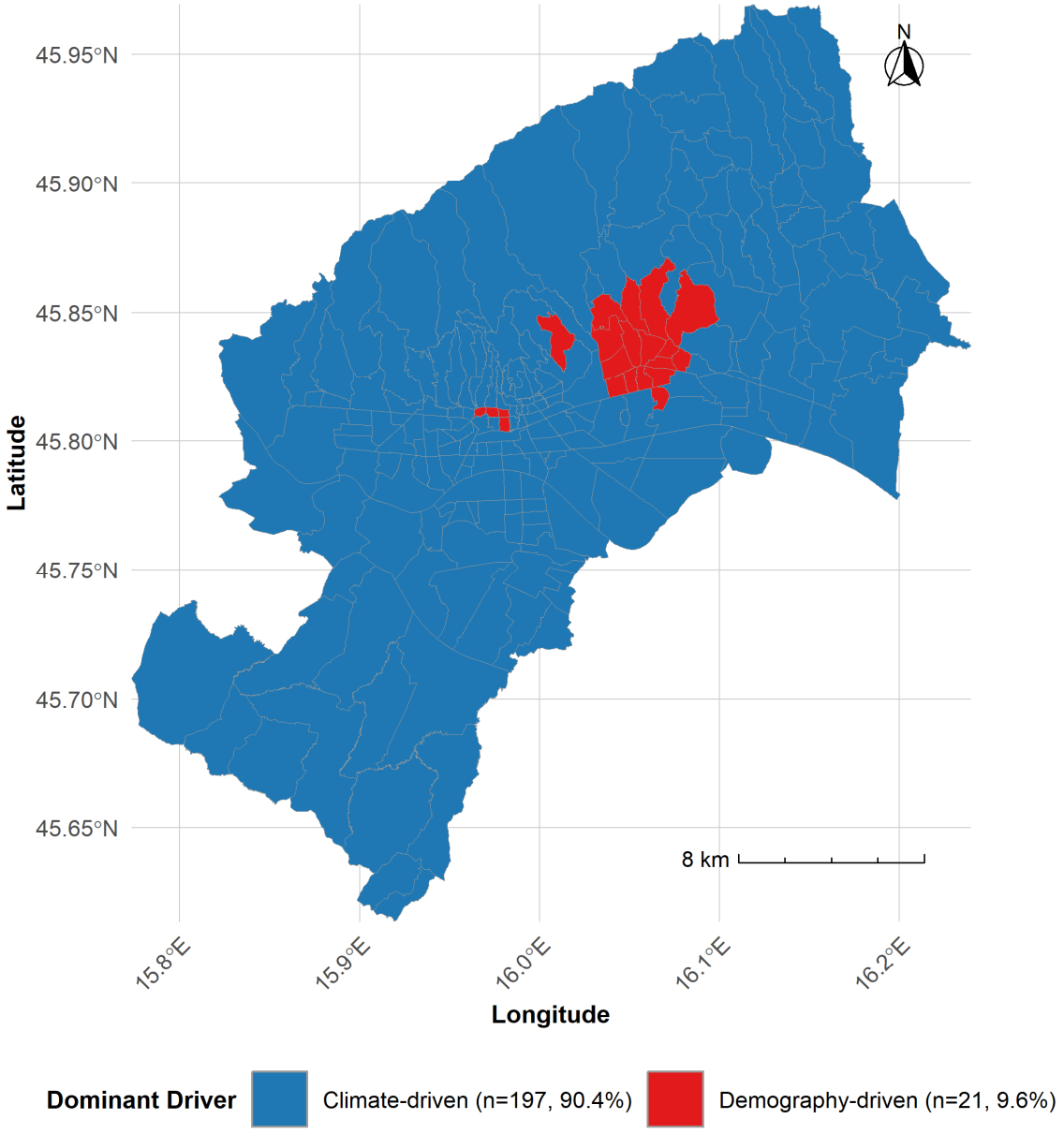


Figure 6. Dominant driver classification map (climate-driven vs. demography-driven neighborhood councils). The classification highlights that most neighborhoods are climate-driven, while a smaller subset of demography-driven areas represents key intervention hotspots.

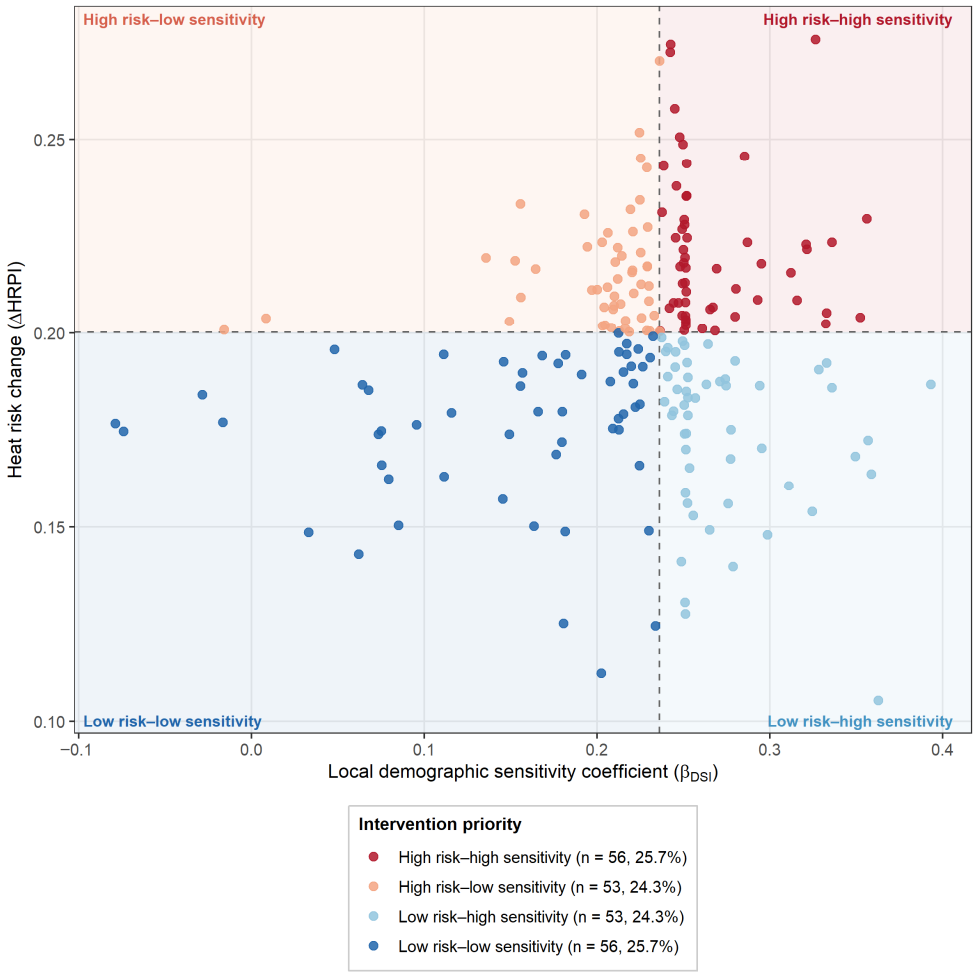


Figure 7. Thermal risk intervention priority matrix based on ΔHRPI and local demographic sensitivity (β_DSI). The matrix identifies priority intervention zones by combining heat risk change and demographic sensitivity, distinguishing critical hotspots from climate-driven and stable areas.

3.4. Sensitivity Checks

The strength of primary findings in the face of alternative methodological choices and data limitations was evaluated by three supplementary analyses. Initially, demographic nonlinearity analysis conducted on 2011 intercensal data demonstrated modest inter-decadal correlations for the change in youth share ($r = -0.176$) and elderly share ($r = +0.123$). Values that are close to zero suggest that the demographic trajectories in Zagreb's post-socialist neighborhood councils lack inter-decadal predictive continuity. The onset of aging was delayed in some neighborhood councils, while others experienced a youth exodus from 2001 to 2011, followed by stabilization or reversal from 2011 to 2021. This nonlinearity affirms that the temporal differencing approach is more suitable than trend extrapolation for the entire 2001–2024 period and provides empirical support for the Method E projection approach implemented.

Secondly, alternative 2024 demographic projections that were based on the 2011–2021 trend periods, rather than the 2001–2021 trend periods, produced nearly identical results (youth: $r = 0.999$; elderly: $r = 0.999$; mean differences near zero: youth -0.0007, elderly -0.0025). This confirms that the core findings are resilient to the selection of projection methods and that the 3-year extrapolation window (2021 → 2024) introduces minimal cumulative uncertainty, irrespective of the reference period used.

Third, the additive HRPI formulation was compared to a multiplicative alternative ([$Tair \times$ LST $\times$ DSI $\times$ Exposure]) using index sensitivity analysis. The Pearson r value was

0.359, and the Spearman ϱ value was 0.312. The top-20 neighborhood council overlap was 20%, and the top-30 neighborhood council overlap was 30%. The rank correlation between additive and multiplicative ΔHRPI was moderate. The modest consistency is indicative of the fundamental differences in aggregation logic: the additive formulation allows for compensatory effects between components, whereas the multiplicative formulation more severely penalizes communities with low values on any single dimension. The additive formulation is maintained because it facilitates transparent linear decomposition and is consistent with vulnerability frameworks that emphasize compensatory capacity. However, practitioners should acknowledge that the identification of priority neighborhood councils is influenced by functional form choices, and the moderate rank correlation is a clear limitation of the current specification.

In spite of these sensitivities, three fundamental findings were consistent across all specifications and robustness checks: (1) HRPI increased significantly citywide from 2001 to 2024; (2) climatic factors dominated city-wide magnitude, while demographic factors dominated spatial differentiation; and (3) local heat risk-driver relationships exhibited substantial spatial heterogeneity, necessitating geographically weighted approaches. The multi-scale heat risk framework presented here is bolstered by the consistency of these patterns across alternative projection methods, index formulations, and modeling specifications.

4. Discussion

This study reveals that the drivers of urban heat risk change operate at distinct spatial scales and that conflating these scales produces misleading conclusions about which factors matter most. Air temperature warming contributed 72% of the city-wide mean HRPI change, making it the dominant driver by any magnitude-based measure. Yet this same factor exhibits minimal spatial heterogeneity; all neighborhood councils warmed by approximately 3 °C over the study period, and this therefore explains relatively little about why heat risk intensified more in some neighborhood councils than others. Demographic sensitivity, by contrast, contributed only 2.3% to the city-wide mean, but because demographic change varied dramatically across space, it emerged as the strongest predictor of spatial differentiation (partial r = 0.677 vs. 0.524 for the strongest climatic factor). These results are not contradictory; they reflect the fundamental distinction between what drove aggregate change citywide and what determined where that change was most severe.

This distinction between magnitude-based drivers and spatial differentiation is increasingly recognized in urban heat vulnerability research, where climatic factors often dominate aggregate trends, while socio-demographic factors explain intra-urban variability [6,7].

The demographic dominance finding aligns with, and extends, the post-socialist urban transition literature. Zagreb's spatial pattern of demographic change reflects the convergence of below-replacement fertility, EU-accession-era youth out-migration toward Western European labor markets, and aging-in-place within socialist-era mass housing complexes originally allocated to young families in the 1970s–1980s. As these cohorts aged simultaneously, demographic sensitivity increased in tandem across contiguous southeastern estates (Dugave, Travno, Sloboština), producing the strong spatial clustering in both ΔDSI and local β_DSI coefficients documented here. This differs from gradual, diffuse aging patterns observed in Western European cities and suggests that post-socialist urban contexts generate particularly pronounced spatial heterogeneity in demographic heat risk, a pattern likely applicable to comparable cities in Poland, Czechia, Hungary, and the former Soviet Union undergoing similar structural transitions. This is consistent with prior studies showing that demographic structure, particularly aging populations, plays a key role in shaping spatial patterns of heat vulnerability within cities [8,20].

The GWR analysis adds a further layer of spatial nuance absent from global models. Local β_DSI coefficients varied by a factor of five across the city (range: −0.079 to +0.393), with the highest values concentrated in southeastern estates and the lowest in central gentrifying districts. This heterogeneity indicates that the same demographic aging process translates into substantially different heat risk consequences depending on the local built environment and adaptive infrastructure context; poor housing quality, limited air conditioning, and inadequate elderly services amplify vulnerability in estates, while higher socioeconomic status attenuates it in central zones. Similar spatial variability in coefficient estimates has been widely documented in GWR-based urban climate studies, where relationships between environmental and socio-demographic variables and temperature outcomes vary substantially across space [44–47].

These spatially distinct amplification and buffering effects suggest the existence of mediating pathways that systematically shape the translation of demographic aging into heat risk. High-β_DSI zones, predominantly situated within southeastern socialist-era estates, probably reflect a convergence of structural vulnerabilities. These encompass thermally inefficient pre-fabricated building stock, low rates of private air conditioning adoption, and restricted access to urban green infrastructure. Low-β_DSI zones in central gentrifying districts, by contrast, likely benefit from a combination of higher private adaptive capacity, proximity to parks and tree-canopied streets, and denser community service provision. Testing these mediating pathways directly through multilevel models incorporating building thermal performance registers, green space accessibility indices, and social service coverage data represents a clear and tractable research agenda that the present GWR coefficient maps are well positioned to motivate.

The absence of significant residual spatial autocorrelation in GWR Model 1c residuals (Moran's I = 0.050, p = 0.089) confirms that this spatially varying coefficient framework adequately captured the underlying structural relationships.

Partial correlation analysis controls for confounding between ΔDSI and climatic predictors; a residual endogeneity concern warrants acknowledgment: DSI is a constituent of HRPI, meaning that some mechanical co-movement exists by construction. The auxiliary regression (ΔDSI~ΔT_{air} + ΔLST, Adj. R^2 = 0.029) confirms that demographic change is largely orthogonal to thermal change, and residual Moran's I on ΔDSI residuals (I = 0.142) confirms that the dominant unexplained variance in demographic change reflects spatially structured socio-demographic processes rather than thermal forcing. Nevertheless, the partial correlation result (r = 0.677) should be interpreted as reflecting the spatial alignment between demographic restructuring and heat risk patterns, not as evidence of a causal demographic-to-risk pathway independent of index construction.

Policy implications follow directly from the multi-scale structure of findings. Universal climate adaptation measures such as urban greening, cool surface deployment, and heat-wave early warning systems address the common thermal forcing and should proceed citywide. Demographic interventions such as elderly support services, age-friendly neighborhood council redesign, and youth retention incentives require spatial precision: the 21 demography-driven neighborhood councils and high-β_DSI zones identified through GWR represent areas where such measures yield disproportionate heat risk reductions per unit investment.

In particular, high β_DSI zones identified through GWR, where demographic sensitivity strongly amplifies heat risk, require targeted interventions focused on elderly populations, including expansion of community-based support services, retrofitting of thermally inefficient housing, and improved access to cooling infrastructure. In contrast, climate-driven areas, where heat risk increases are primarily driven by temperature change,

are more effectively addressed through universal measures such as urban greening, surface albedo modification, and city-wide heat warning systems.

For example, a municipal planning strategy could prioritize southeastern high β_DSI neighborhood councils for integrated intervention packages combining building retrofits, establishment of cooling centers, and targeted elderly outreach programs, while simultaneously implementing citywide greening and heat mitigation strategies to address the broader thermal baseline. In this way, GWR-derived spatial patterns can be directly translated into differentiated planning actions, improving both efficiency and equity of urban heat adaptation.

Deploying demographic programs uniformly across all 218 neighborhood councils would substantially dilute their impact. GWR-derived coefficient maps provide the spatial targeting infrastructure necessary for efficient allocation of limited adaptation resources, a methodological contribution directly applicable to urban heat governance in comparable post-socialist cities.

While this study offers a strong framework for separating the effects of climate and population on urban heat risk, some limitations should be acknowledged when interpreting the results, particularly regarding detailed vulnerability and health impacts. For example, using air temperature data with a relatively low resolution (CERRA) might hide small-scale temperature differences that are important at the neighborhood level.

Similarly, demographic projections are constrained by data availability and could be refined in future work through more advanced cohort-based or dynamic modeling approaches. In addition, the absence of socioeconomic and adaptive capacity indicators means that the HRPI should be interpreted as an exposure-sensitivity measure rather than a comprehensive vulnerability index. Factors such as income, housing quality, access to cooling, and social support networks—known to shape adaptive capacity—are not captured in the current framework.

From a thermal standpoint, the employment of land surface and air temperature as proxies fails to comprehensively capture physiological heat stress; a more direct assessment could be achieved through indices like the Universal Thermal Climate Index (UTCI). Ultimately, the absence of validation against health outcome data, including mortality rates or hospital admissions, constrains the capacity to directly correlate modeled heat risk with observed impacts.

Addressing these limitations is a key area for future research. This will help improve the thoroughness of heat vulnerability assessments and make the framework more useful for public health and urban planning.

An important avenue for future research is the extension of the present two-period framework into a multi-temporal panel structure. While the current design enables clear separation of spatial variance and scale-dependent drivers, incorporating additional temporal points would allow for explicit modeling of temporal trajectories and path dependencies in heat risk dynamics. In particular, Bayesian spatiotemporal modeling approaches may provide a more flexible framework for capturing both spatial heterogeneity and temporal evolution, especially in rapidly transforming post-socialist urban contexts. The availability of historical census and thermal data makes such extensions feasible and represents a logical next step, building directly on the present analysis.

5. Limitations

This study advances the methodological and empirical understanding of spatiotemporal heat risk change in post-socialist cities, but several limitations constrain the scope of inference and suggest directions for future research.

- Thermal data resolution. CERRA reanalysis of air temperature data at 5.5 km horizontal resolution may underestimate microclimatic variability at the neighborhood council scale, particularly in topographically complex zones along the Medvednica slope. Validation against Zagreb meteorological station data confirmed acceptable correspondence, but sub-kilometer atmospheric temperature fields, which are currently unavailable for the full 2001–2024 period, would strengthen the thermal component of the HRPI.
- Demographic projection uncertainty. Age-structure shares for 2024 were held constant from 2021 census values (Method E), which outperformed trend extrapolation in retrospective validation but assumes demographic stability over the 2021–2024 window. Neighborhood councils are experiencing abrupt post-2021 shifts.
- Partial vulnerability framework. The HRPI characterizes the exposure-sensitivity dimension of heat vulnerability but excludes adaptive capacity indicators (income, housing quality, air conditioning access, social networks) unavailable at the miesni odbor level in Croatian census data. Neighborhood councils identified as high-risk may therefore include populations with substantial private adaptive resources that partially offset thermal and demographic exposure. Integration of socioeconomic indicators from administrative registers or survey data would substantially strengthen vulnerability characterization.
- Thermal metric coverage. LST captures surface-level microclimate conditions but does not directly represent physiological heat stress, which additionally depends on humidity, wind speed, nocturnal cooling rates, and heat-wave duration and frequency. Future work incorporating apparent temperature or UTCI indices alongside LST would improve epidemiological relevance.
- Absence of health outcome validation. HRPI cannot be externally validated against heat-related morbidity or mortality data, as such records are unavailable at neighborhood council resolution in Croatia. Validation against hospital admission or excess mortality data, as more granular health surveillance infrastructure develops, remains a priority for confirming that index-derived risk rankings correspond to actual health outcomes.

6. Conclusions

Urban heat risk in Zagreb increased substantially and universally between 2001 and 2024, with all 218 neighborhood councils recording positive ΔHRPI. The principal finding of this study is that the drivers of this increase operate at fundamentally different spatial scales and that the scale of analysis determines which factor appears dominant. Regional air temperature warming, a near-uniform forcing of approximately +3 °C, drove the largest share of city-wide mean change. Spatially differentiated demographic restructuring—youth out-migration and aging-in-place concentrated in southeastern post-socialist housing estates—determined which neighborhood councils experienced disproportionate increases. At the local level, geographically weighted regression revealed that the strength of both demographic and thermal effects varies continuously across the city, with coefficient heterogeneity that global models structurally cannot represent.

The composite Demographic Sensitivity Index outperformed disaggregated age components in GWR specifications, supporting the interpretation that heat risk operates as an emergent property of neighborhood council age structure rather than a simple additive function of youth and elderly shares. This finding, combined with the strong spatial clustering of local β_DSI coefficients (Moran's I = 0.647), suggests that the contextual built environment—housing quality, adaptive infrastructure, and social service provision—systematically amplifies or attenuates the translation of demographic aging

into heat risk. These contextual interpretations should be read as plausible mechanisms consistent with the mapped spatial structure, but the GWR results themselves remain associational. The value of the local modeling is to reveal where demographic restructuring aligns most strongly with risk change and to motivate targeted data collection and intervention design in those zones rather than claim definitive causal pathways. The southeastern socialist-era estates, where high demographic sensitivity coincides with poor thermal infrastructure and low adaptive capacity, represent the highest-priority zones for integrated intervention.

Methodologically, the multi-scale framework developed here, combining additive index decomposition, partial correlation analysis, and geographically weighted regression, provides a replicable approach for disentangling magnitude-based from variance-based drivers of vulnerability change. It is directly applicable to other post-socialist cities undergoing simultaneous climate warming and demographic restructuring, where the spatial concentration of aging populations in socialist-era housing stock is likely to generate comparable patterns of spatially heterogeneous heat risk. As 2024 marked the hottest year on record globally, frameworks capable of identifying not merely that heat risk is rising but precisely where and through which mechanisms are an urgent precondition for efficient and equitable urban adaptation.

Overall, the findings highlight three key insights: (1) urban heat risk is increasing universally but unevenly across neighborhood councils; (2) climatic factors dominate city-wide magnitude, while demographic restructuring explains spatial differentiation; and (3) local-scale heterogeneity requires spatially targeted, rather than uniform, adaptation strategies. These insights provide a concise framework for interpreting heat risk dynamics and support more effective, evidence-based urban planning responses.

Author Contributions: Conceptualization, D.B. and M.G.; methodology, D.B. and M.G.; software, D.B.; validation, D.B. and M.G.; formal analysis, D.B.; investigation, D.B.; resources, D.B.; data curation, D.B. and M.G.; writing—original draft preparation, D.B.; writing—review and editing, M.G.; visualization, D.B.; supervision, M.G.; project administration, D.B. and M.G.; funding acquisition, M.G. All authors have read and agreed to the published version of the manuscript.

Funding: This study was supported by the Croatian Science Foundation for the ALCAR project "Assessment of the Long-term Climatic and Anthropogenic Effects on the Spatio-temporal Vegetated Land Surface Dynamics in Croatia using Earth Observation Data" (Grant No. HRZZ IP-2022-10-5711).

Data Availability Statement: The Landsat surface temperature data used in this study are publicly available from the United States Geological Survey (USGS) EarthExplorer platform. Atmospheric temperature data from the Copernicus Regional Reanalysis for Europe (CERRA) are openly accessible through the Copernicus Climate Data Store. Neighborhood council-level demographic data for Zagreb (2001, 2021) were obtained from the City of Zagreb and are not publicly shareable due to national data-use and licensing restrictions. Derived demographic indicators (PVI, ΔPVI) and spatial units are therefore available only in aggregated form. The processed datasets generated during this study—LST layers, UHI-PVI indices for 2001 and 2024, temporal difference layers (ΔLST, ΔUHI-PVI), and GWR model outputs—are available from the corresponding author upon reasonable request.

Conflicts of Interest: The authors declare no conflicts of interest.

References

1. IPCC. *Climate Change 2022: Impacts, Adaptation and Vulnerability*; Cambridge University Press: Cambridge, UK, 2022.
2. Oke, T.R. The energetic basis of the urban heat island. *Q. J. R. Meteorol. Soc.* **1982**, *108*, 1–24. [CrossRef]
3. Copernicus Climate Change Service (C3S); World Meteorological Organization (WMO). *European State of the Climate 2024*; WMO: Geneva, Switzerland, 2025. [CrossRef]
4. Bečić, D.; Gašparović, M. Urban heat islands and land-use patterns in Zagreb: A composite analysis using remote sensing and spatial statistics. *Land* **2025**, *14*, 1470. [CrossRef]

5. Reid, C.E.; O'Neill, M.S.; Gronlund, C.J.; Brines, S.J.; Brown, D.G.; Diez-Roux, A.V.; Schwartz, J. Mapping community determinants of heat vulnerability. *Environ. Health Perspect.* **2009**, *117*, 1730–1736. [CrossRef]
6. Niu, Y.; Li, Z.; Gao, Y.; Liu, X.; Xu, L.; Vardoulakis, S.; Yue, Y.; Wang, J.; Liu, Q. A systematic review of the development and validation of the heat vulnerability index: Major factors, methodologies, and gaps. *Curr. Clim. Change Rep.* **2021**, *7*, 87–97. [CrossRef]
7. Wang, C.; Chang, H.-T. Hotspots, heat vulnerability and urban heat islands: An interdisciplinary review of research methodologies. *Can. J. Remote Sens.* **2020**, *46*, 532–551. [CrossRef]
8. Ramly, N.; Hassan, M.R.; Jaafar, M.H.; Ismail, R.; Isa, Z.; Hod, R. Identifying vulnerable population in urban heat island: A literature review. *Int. J. Public Health Res.* **2023**, *13*, 1678–1693. [CrossRef]
9. Zhan, W.; Bechtel, B.; Du, H.; Chakraborty, T.C.; Kotthaus, S.; Krayenhoff, E.S.; Martilli, A.; Naserikia, M.; Nazarian, N.; Roth, M.; et al. Satellite-derived land surface temperatures strongly mischaracterise urban heat hazard. *Nat. Cities* **2025**, *1*, 45–57. [CrossRef]
10. Li, F.; Yigitcanlar, T.; Li, W.; Nepal, M.; Nguyen, K.; Dur, F. Understanding urban heat vulnerability: Scientometric analysis of five decades of research. *Urban Clim.* **2024**, *56*, 102035. [CrossRef]
11. Conlon, K.C.; Mallen, E.; Gronlund, C.J.; Berrocal, V.J.; Larsen, L.; O'Neill, M.S. Mapping human vulnerability to extreme heat: A critical assessment of heat vulnerability indices created using principal components analysis. *Environ. Health Perspect.* **2020**, *128*, 077002. [CrossRef]
12. Bao, J.; Li, X.; Yu, C. The construction and validation of the heat vulnerability index, a review. *Int. J. Environ. Res. Public Health* **2015**, *12*, 7220–7234. [CrossRef]
13. Derakhshan, S.; Eisenman, D.P.; Basu, R.; Longcore, T. Do social vulnerability indices correlate with extreme heat health outcomes? *J. Clim. Change Health* **2024**, *18*, 100276. [CrossRef]
14. Alnajjar, S.; García-Martínez, A.; López-Cabeza, V.P.; Al-Azhari, W. A multidimensional approach to mapping urban heat vulnerability: Integrating remote sensing and spatial configuration. *Smart Cities* **2025**, *8*, 105814. [CrossRef]
15. Li, F.; Yigitcanlar, T.; Nepal, M.; Nguyen, K.; Dur, F.; Li, W. Assessing heat vulnerability and multidimensional inequity: Lessons from indexing the performance of Australian capital cities. *Sustain. Cities Soc.* **2024**, *115*, 105875. [CrossRef]
16. Voelkel, J.; Hellman, D.; Sakuma, R.; Shandas, V. Assessing Vulnerability to Urban Heat: A Study of Disproportionate Heat Exposure and Access to Refuge by Socio-Demographic Status in Portland, Oregon. *Int. J. Environ. Res. Public Health* **2018**, *15*, 640. [CrossRef]
17. Mushore, T.D.; Mutanga, O.; Odindi, J.; Dube, T. Determining extreme heat vulnerability of Harare Metropolitan City using multispectral remote sensing and socio-economic data. *J. Spat. Sci.* **2018**, *63*, 173–191. [CrossRef]
18. Ascencio, E.J.; Barja, A.; Benmarhnia, T.; Carrasco-Escobar, G. Disproportionate exposure to surface-urban heat islands across vulnerable populations in Lima city, Peru. *Environ. Res. Lett.* **2023**, *18*. [CrossRef]
19. Gabbe, C.J.; Pierce, G. Extreme Heat Vulnerability of Subsidized Housing Residents in California. *Hous. Policy Debate* **2020**, *30*, 843–860. [CrossRef]
20. Gronlund, C.J. Racial and Socioeconomic Disparities in Heat-Related Health Effects and Their Mechanisms: A Review. *Curr. Epidemiol. Rep.* **2014**, *1*, 165–173. [CrossRef] [PubMed]
21. Loughnan, M.; Nicholls, N.; Tapper, N.J. Mapping Heat Health Risks in Urban Areas. *Int. J. Popul. Res.* **2012**, *2012*, 518687. [CrossRef]
22. Navarro-Estupiñan, J.; Robles-Morua, A.; Díaz-Caravantes, R.; Vivoni, E.R. Heat risk mapping through spatial analysis of remotely-sensed data and socioeconomic vulnerability in Hermosillo, México. *Urban Clim.* **2020**, *34*, 100682. [CrossRef]
23. Kang, S.; Lee, D.; Park, J.; Jung, J. Exploring Urban Forms Vulnerable to Urban Heat Islands: A Multiscale Analysis. *Sustainability* **2022**, *14*, 3603. [CrossRef]
24. Sestito, B.; Reimann, L.; Mazzoleni, M.; Botzen, W.J.; Aerts, J. Identifying vulnerability factors associated with heatwave mortality: A spatial statistical analysis across Europe. *Environ. Res. Lett.* **2025**, *20*, 044025. [CrossRef]
25. Ho, H.C.; Tong, S.; Zhou, Y.; Hu, K.; Yang, X.; Yang, Y. Mapping Heat Vulnerability and Heat Risk for Neighborhood Health Risk Management in Urban Environment? Challenges and Opportunities. *Curr. Environ. Health Rep.* **2025**, *12*, 14. [CrossRef]
26. Dongo, K.; Kablan, A.K.M.; Kouamé, F.K. Mapping Urban Residents' Vulnerability to Heat in Abidjan, Côte d'Ivoire. *Clim. Dev.* **2018**, *10*, 600–613. [CrossRef]
27. Weber, S.; Sadoff, N.; Zell, E.; de Sherbinin, A. Policy-relevant indicators for mapping the vulnerability of urban populations to extreme heat events: A case study of Philadelphia. *Appl. Geogr.* **2015**, *63*, 231–243. [CrossRef]
28. Jia, R.; Liu, J.; He, T.; Han, D.; Xu, X.; Liu, L.; Sun, Z.; Qiao, Z. Population heat exposure risk from the perspective of urban heat island spatial expansion in China during 2005-2020. *Urban Clim.* **2021**, *56*, 101987. [CrossRef]
29. Grigorescu, I.; Mocanu, I.; Mitrică, B.; Dumitraşcu, M.; Dumitrică, C.; Dragotă, C.-S. Socio-economic and environmental vulnerability to heat-related phenomena in Bucharest metropolitan area. *Environ. Res.* **2021**, *192*, 110268. [CrossRef] [PubMed]

30. Parker, C.; Mahlasi, C.; Govindasamy, T.; Radebe, L.; Brink, N.B.; Jack, C.; Doumbia, M.; Kouakou, E.; Chersich, M.; Chersich, M.; et al. Publisher Correction: Quantifying Intra-Urban Socio-Economic and Environmental Vulnerability to Extreme Heat Events in Johannesburg, South Africa. *Int. J. Biometeorol.* **2025**, *69*, 2519. [CrossRef]
31. Fung, K.Y.; Yang, Z.-L.; Martilli, A.; Krayenhoff, E.S.; Niyogi, D. Prioritizing social vulnerability in urban heat mitigation. *PNAS Nexus* **2024**, *3*. [CrossRef]
32. Mashhoodi, B. Temperature Rise Amplifies Environmental Inequities? Europe's North-South Divide. *Appl. Spat. Anal. Policy* **2024**, *17*, 599–617. [CrossRef]
33. Liu, D.; Zhou, R.; Ma, Q.; He, T.; Fang, X.; Xiao, L.; Hu, Y.; Li, J.; Shao, L.; Gao, J. Spatio-temporal patterns and population exposure risks of urban heat island in megacity Shanghai, China. *Sustain. Cities Soc.* **2024**, *108*, 105500. [CrossRef]
34. Sánchez-Guevara Sánchez, C.; Núñez Peiró, M.; Neila González, F.J. Urban Heat Island and Vulnerable Population. The Case of Madrid. In *Sustainable Development and Renovation in Architecture, Urbanism and Engineering*; Mercader-Moyano, P., Ed.; Springer: Berlin/Heidelberg, Germany, 2017; pp. 3–13. [CrossRef]
35. Badakhshan, B.; Sharifi, A.; Karami, T.; Salehipour Bavarsad, F. Urban heat in a very hot region: Exploring spatial inequality in exposure to extreme heat hazard in Tehran, Iran. *Urban Clim.* **2025**, *61*, 102480. [CrossRef]
36. Moreira, A.B.; Nobrega, R.S.; Wanderley, L.S.A.; Matzarakis, A. Urban Heat Island Vulnerability in the City of Recife, Pernambuco, Brazil. *Weather Clim. Soc.* **2024**, *16*, 105–116. [CrossRef]
37. Krenz, K.; Amann, L. Urban Heat Island Effect: Examining Spatial Patterns of Socio-Demographic Inequalities in Greater London. *Cities Health* **2025**, *9*, 901–924. [CrossRef]
38. Quintana-Talvac, C.; Corvacho-Ganahin, O.; Smith, P.; Sarricolea, P.; Prieto, M.; Meseguer-Ruiz, O. Urban heat islands and vulnerable populations in a mid-size coastal city in an arid environment. *Atmosphere* **2021**, *12*, 917. [CrossRef]
39. Barrera Alarcón, I.; Tapia-McClung, R.; Caudillo Cos, C.; Arvizu Piña, V.; Montejano-Escamilla, J.A. Vulnerable population and risk areas to the surface urban heat island phenomenon and their accessibility to healthcare: The 15 warmest Mexican cities. *Int. J. Cartogr.* **2025**, *11*, 358–387. [CrossRef]
40. Wu, C.; Shui, W.; Huang, Z.; Wang, C.; Wu, Y.; Wu, Y.; Xue, C.; Huang, Y.; Zhang, Y.; Zheng, D. Urban heat vulnerability: A dynamic assessment using multi-source data in coastal metropolis of Southeast China. *Front. Public Health* **2022**, *10*, 989963. [CrossRef]
41. Česić, M.; Rogulj, K.; Krtalić, A. Combined Thermal Index Development for Urban Heat Island Detection in Area of Split, Croatia. *Land* **2025**, *14*, 175. [CrossRef]
42. Habib, M.M.; van Esch, M.; van Ham, M.; Timmermans, W.J. High-resolution datasets for urban heat vulnerability assessment in urbanized areas of the Netherlands. *Data Brief* **2025**, *60*, 111525. [CrossRef] [PubMed]
43. Jalalzadeh Fard, B.; Mahmood, R.; Hayes, M.; Rowe, C.; Abadi, A.M.; Shulski, M.; Bell, J.E. Mapping heat vulnerability index based on different urbanization levels in Nebraska, USA. *GeoHealth* **2021**, *5*, e2021GH000478. [CrossRef]
44. Ivajnšič, D.; Kaligarič, M.; Žiberna, I. Geographically weighted regression of the urban heat island of a small city. *Appl. Geogr.* **2014**, *53*, 341–353. [CrossRef]
45. Ünsal, Ö.; Lotfata, A.; Avcı, S. Exploring the relationships between land surface temperature and its influencing determinants using local spatial modeling. *Sustainability* **2023**, *15*, 11594. [CrossRef]
46. Zhao, C.; Jensen, J.; Weng, Q.; Weaver, R. A geographically weighted regression analysis of the underlying factors related to the surface urban heat island phenomenon. *Remote Sens.* **2018**, *10*, 1428. [CrossRef]
47. Wang, Z.; Fan, C.; Zhao, Q.; Myint, S.W. A geographically weighted regression approach to understanding urbanization impacts on urban warming and cooling: A case study of Las Vegas. *Remote Sens.* **2020**, *12*, 222. [CrossRef]
48. Comber, A.; Brunsdon, C.; Charlton, M.; Dong, G.; Harris, R.; Lu, B.; Lü, Y.; Murakami, D.; Nakaya, T.; Wang, Y.; et al. A route map for successful applications of geographically weighted regression. *Geogr. Anal.* **2023**, *55*, 155–178. [CrossRef]
49. Sidiqui, P.; Roös, P.B.; Herron, M.; Jones, D.S.; Duncan, E.; Jalali, A.; Allam, Z.; Roberts, B.J.; Schmidt, A.; Tariq, M.A.U.R.; et al. Urban Heat Island vulnerability mapping using advanced GIS data and tools. *J. Earth Syst. Sci.* **2022**, *131*, 266. [CrossRef]
50. He, X.; Yuan, Q.; Qin, Y.; Lu, J.; Li, G. Analysis of surface urban heat island in the Guangzhou-Foshan metropolitan area based on local climate zones. *Land* **2024**, *13*, 1626. [CrossRef]
51. Heaviside, C.; Macintyre, H.; Vardoulakis, S. The Urban Heat Island: Implications for health in a changing environment. *Curr. Environ. Health Rep.* **2017**, *4*, 517–523. [CrossRef]
52. Técher, M.; Ait Haddou, H.; Aguejdad, R. Urban Heat Island's vulnerability assessment by integrating urban planning policies: A case study of Montpellier Méditerranée Metropolitan Area, France. *Sustainability* **2023**, *15*, 1820. [CrossRef]
53. Williams, A.A.; Allen, J.G.; Catalano, P.J.; Spengler, J.D. The role of individual and small-area social and environmental factors on heat vulnerability to mortality within and outside of the home in Boston, MA. *Climate* **2020**, *8*, 29. [CrossRef]
54. Zhang, X.; Ye, R.; Fu, X. Assessment of urban local high-temperature disaster risk and the spatially heterogeneous impacts of blue-green space. *Atmosphere* **2023**, *14*, 1652. [CrossRef]

55. Guardaro, M.; Hondula, D.M.; Redman, C.L. Social capital: Improving community capacity to respond to urban heat. *Local Environ.* **2022**, *27*, 1133–1150. [CrossRef]
56. Tieskens, K.F.; Smith, I.A.; Jimenez, R.B.; Hutyra, L.R.; Fabian, M.P. Mapping the gaps between cooling benefits of urban greenspace and population heat vulnerability. *Sci. Total Environ.* **2022**, *845*, 157283. [CrossRef]
57. Puntub, W.; Schnittfinke, T.; Fleischhauer, M.; Birkmann, J.; Garschagen, M.; Sandholz, S.; Wannewitz, M. Linking Science and Practice in Participatory Future-Oriented Assessment and Planning of Human Heat Stress Vulnerability in Bonn, Germany. *J. Environ. Plan. Manag.* **2023**, *66*, 1918–1937. [CrossRef]
58. Jonsson, A.C.; Lundgren, L. Vulnerability and Adaptation to Heat in Cities: Perspectives and Perceptions of local adaptation decision-makers in Sweden. *Local Environ.* **2014**, *20*, 442–458. [CrossRef]
59. Copernicus Climate Change Service (C3S). Summer 2024—Hottest on Record Globally and in Europe. 2024. Available online: https://climate.copernicus.eu (accessed on 15 May 2025).
60. Copernicus. Observer: Europe's Warmest Year on Record—Striking Climate Contrasts in 2024. 2024. Available online: https://www.copernicus.eu (accessed on 28 May 2025).
61. Državni hidrometeorološki zavod (DHMZ). Ocjena Mjeseca Kolovoza 2024. 2024. Available online: https://meteo.hr (accessed on 28 May 2025).
62. Copernicus Climate Change Service (C3S). Copernicus European Regional Reanalysis (CERRA) [Data set]. 2021. Available online: https://cds.climate.copernicus.eu/ (accessed on 28 May 2025).
63. Schimanke, S.; Möller, J.; Undén, P.; Bazile, E. CERRA sub-daily regional reanalysis data for Europe on single levels from 1984 to present. In *Copernicus Climate Change Service (C3S) Climate Data Store (CDS)*; ECMWF: Reading, UK, 2021. [CrossRef]
64. Manapragada, N.V.S.K.; Mandelmilch, M.; Roitberg, E.; Kizel, F.; Natanian, J. Remote Sensing for Environmentally Responsive Urban Built Environment: A Review of Tools, Methods and Gaps. *Remote Sens. Appl. Soc. Environ.* **2025**, *38*, 101529. [CrossRef]
65. Venter, Z.S.; Krog, N.H.; Barton, D.N. Linking Green Infrastructure to Urban Heat and Human Health Risk Mitigation in Oslo, Norway. *Sci. Total Environ.* **2020**, *709*, 136193. [CrossRef]
66. Državni Zavod za Statistiku. Popis Stanovništva, Kućanstava i Stanova 2001. 2001. Available online: https://web.dzs.hr/Eng/censuses/Census2001/census.htm (accessed on 1 December 2025).
67. Državni zavod za statistiku. Popis stanovništva, kućanstava i stanova 2021. 2021. Available online: https://podaci.dzs.hr/en/statistics/population/census/ (accessed on 1 December 2025).
68. Xu, Z.; Etzel, R.A.; Su, H.; Huang, C.; Guo, Y.; Tong, S. Impact of ambient temperature on children's health: A systematic review. *Environ. Res.* **2012**, *117*, 120–131. [CrossRef]
69. Fouillet, A.; Rey, G.; Laurent, F.; Pavillon, G.; Bellec, S.; Guihenneuc-Jouyaux, C.; Clavel, J.; Jougla, E.; Hémon, D. Excess mortality related to the August 2003 heat wave in France. *Int. Arch. Occup. Environ. Health* **2006**, *80*, 16–24. [CrossRef] [PubMed]
70. Basu, R.; Samet, J.M. Relation between elevated ambient temperature and mortality: A review of the epidemiologic evidence. *Epidemiol. Rev.* **2002**, *24*, 190–202. [CrossRef]
71. Åström, D.O.; Forsberg, B.; Rocklöv, J. Heat wave impact on morbidity and mortality in the elderly population: A review of recent studies. *Maturitas* **2011**, *69*, 99–105. [CrossRef] [PubMed]
72. Smit, B.; Wandel, J. Adaptation, adaptive capacity and vulnerability. *Glob. Environ. Change* **2006**, *16*, 282–292. [CrossRef]
73. Birkmann, J. (Ed.) *Measuring Vulnerability to Natural Hazards: Towards Disaster Resilient Societies*; United Nations University Press: Tokyo, Japan, 2006.
74. Rocha, R.B.; Ribeiro, H. A Heat Vulnerability Index: Spatial Patterns of Exposure, Sensitivity and Adaptive Capacity for Santiago de Chile. *PLoS ONE* **2016**, *11*, e0162464. [CrossRef]
75. Harlan, S.L.; Brazel, A.J.; Prashad, L.; Stefanov, W.L.; Larsen, L. Neighborhood Microclimates and Vulnerability to Heat Stress. *Soc. Sci. Med.* **2006**, *63*, 2847–2863. [CrossRef]
76. Wolf, T.; McGregor, G.; Analitis, A. Performance assessment of a heat wave vulnerability index for Greater London, United Kingdom. *Weather Clim. Soc.* **2010**, *2*, 32–46. [CrossRef]
77. Kendall, M.G.; Stuart, A. *The Advanced Theory of Statistics*; Griffin: London, UK, 1961; Volume 2.
78. Brunsdon, C.; Fotheringham, A.S.; Charlton, M.E. Geographically Weighted Regression: A Method for Exploring Spatial Nonstationarity. *Geogr. Anal.* **1996**, *28*, 281–298. [CrossRef]
79. Fotheringham, A.S.; Brunsdon, C.; Charlton, M. *Geographically Weighted Regression: The Analysis of Spatially Varying Relationships*; Wiley: Chichester, UK, 2002.
80. Burnham, K.P.; Anderson, D.R. *Model Selection and Multimodel Inference: A Practical Information-Theoretic Approach*, 2nd ed.; Springer: New York, NY, USA, 2002.

Disclaimer/Publisher's Note: The statements, opinions and data contained in all publications are solely those of the individual author(s) and contributor(s) and not of MDPI and/or the editor(s). MDPI and/or the editor(s) disclaim responsibility for any injury to people or property resulting from any ideas, methods, instructions or products referred to in the content.